remote sensing

MDPI

Article

Environmental Degradation in Iraq: Attribution of Climatic Change and Human Influences Through Multi-Factor Analysis

Akram Alqaraghuli [1,2,3,*], Peter North [1], Iain Bye [1], Jacqueline Rosette [1] and Sietse Los [1,4]

[1] Global Environmental Modelling and Earth Observation (GEMEO), Department of Geography, Faculty of Science and Engineering, Swansea University, Singleton Park, Swansea SA2 8PP, UK; p.r.j.north@swansea.ac.uk (P.N.); i.j.bye@swansea.ac.uk (I.B.); j.a.rosette@swansea.ac.uk (J.R.); s.o.los@swansea.ac.uk (S.L.)
[2] Civil Engineering Department, Swansea University, Fabian Way, Swansea SA1 8EN, UK
[3] Engineering Affairs Department, Iraqi Ministry of Justice, Administrative and Financial Department, Haifa Street, Baghdad Al-Salehiyah, Baghdad 10001, Iraq
[4] Wetland Conservation Unit, Wildfowl and Wetlands Trust, Slimbridge GL2 7BT, UK
* Correspondence: 2013625@swansea.ac.uk or akramalqaraghuli89@gmail.com; Tel.: +44-7776802670

Highlights

- Over half (56.5%) of Thi-Qar's vegetation cover showed a decrease from 2001 to 2022, showing widespread degradation.
- Regression analysis showed that the NDVI was influenced more by streamflow than by LST or rainfall.
- The strong correlation between the NDVI and streamflow suggests that water management is more critical than climate patterns in preventing land degradation in this region.
- This study presents a replicable model for monitoring the effects of hydrological–climatic interactions on vegetation cover in similar arid places around the globe.

What are the main findings?

- Vegetation degradation is widespread: over half (56.5%) of Thi-Qar experienced vegetation loss from 2001 to 2022, with only 12% of the region showing improvement.
- Streamflow outweighs climate factors: hydrological control, particularly river discharge, is a stronger determinant of vegetation cover than rainfall or temperature, underscoring the importance of human water management as a key driver of land degradation or recovery.

What are the implications of the main findings?

- Water management is critical for land restoration: the strong link between streamflow and the NDVI suggests that improving water distribution and irrigation efficiency could mitigate degradation more effectively than climate adaptation alone.
- A scalable monitoring framework for arid regions: the study provides a replicable, satellite-based model to assess vegetation responses to hydrological and climatic changes, supporting evidence-based policy in vulnerable drylands worldwide.

Abstract

Environmental degradation in Iraq is a critical issue that requires strong monitoring. One indication of land degradation is a decrease in or loss of vegetation cover. This study examines changes in vegetation and productivity in the Thi-Qar region from 2001 to 2022, using the normalized difference vegetation index (NDVI) and net primary production (NPP), and their response to climatic and hydrological factors. To address the gap in assessments that simultaneously quantify the influence of streamflow, rainfall, and temperature

Academic Editor: Gareth Rees

Received: 30 December 2025
Revised: 28 January 2026
Accepted: 13 February 2026
Published: 19 February 2026

across distinct land cover classes in arid and semi-arid regions, we developed a replicable multi-source geospatial framework. We used MODIS data within the Google Earth Engine platform to perform spatiotemporal analysis. We applied models to detect NDVI trends on a pixel-by-pixel basis. This study provides the first integrated, data-driven assessment of vegetation sensitivity to streamflow versus climate in the Thi-Qar Governorate using a harmonized multi-source dataset. This combines the FAO WaPOR NPP dataset with hydrological (streamflow) and climatic (CHIRPS rainfall, MODIS LST) variables within an analytical workflow to extract anthropogenic water management from climatic drivers. The results showed variations in the NDVI and productivity in the southern and southwestern regions, indicating areas of both degradation and improvement. The analysis found that 12% of the study area showed improvement, while 56.5% of the area showed degradation. Additionally, we classified the study area as either vegetation (cropland) or non-vegetation (fallow arable land, bare areas, and sand dunes). A multiple regression model was then applied to these categories to examine the relationships between streamflow, precipitation, land surface temperature (LST), and the NDVI. The multiple regression for the entire region showed that these factors explained 45.1% of NDVI variation, with streamflow being the most significant positive driver ($p < 0.001$). The result showed that the NDVI in cropland and arable land was strongly positively correlated with both precipitation and streamflow (R = 0.78, R = 0.75). In contrast, bare land and dunes showed weaker relationships (R = 0.26 and 0.51, respectively). Of these factors, streamflow had the most significant influence in explaining vegetation change (partial correlation $p = 0.53$), indicating the importance of human management in addition to climate.

Keywords: degradation; NDVI; climate factors; Google Earth Engine (GEE); streamflow; Mann–Kendall

1. Introduction

The Middle East–North Africa (MENA) region is facing some of the world's most severe challenges related to climate change and land degradation. These stressors closely resemble those affecting other arid and semi-arid regions worldwide, such as the Sahel and the southwestern United States [1–3]. Over 70% of permanent surface water loss globally occurs in five countries, including Iraq [4], and highlights the need for international cooperation to manage shared water resources and mitigate climate impacts. Studying the shifting climatic conditions in the Middle East and other regions over an extended period is necessary to assess the current situation and to predict future change. For this, the use of remote sensing techniques combined with statistical analyses offers a replicable framework for assessing vegetation and climatic changes in this and other regions [5,6].

Remote sensing is widely used to study land degradation on regional, continental, and global scales, with land-use change and vegetation index measures as the most common indicators [5,7]. The normalized difference vegetation index (NDVI) is widely used to study the spatial–temporal evolution trends in vegetation cover, since it is sensitive to vegetation cover and productivity, and reduces errors caused by variation in instrument calibration, solar angle, terrain, cloud shadows, and soil color [8–10]. Subsequent advances emphasized the need for multi-indicator frameworks. For example [11], the four remote sensing indicators—vegetation cover, runoff, soil erosion, and rain use efficiency (RUE)—were integrated to create a desertification monitoring system for sub-Saharan Africa, demonstrating that no single index could fully capture the complex process of land degradation. This emphasizes the necessity of multivariate, long-term monitoring.

Further studies in the field have involved linking physical environmental changes with hydrological and human-related factors. Studies such as [12] applied the Dahlem Desertification Paradigm (DDP) to understand how hydrology connects biophysical and socio-economic factors, while [13] used hydrological modeling to quantify how land cover change (e.g., deforestation) directly alters basin-scale water balance and runoff. More recently, the advent of cloud-computing platforms like Google Earth Engine (GEE) has enabled continent- and regional-scale spatiotemporal analyses. For example, vegetation dynamics across South Asia from 2001 to 2023 have been analyzed using MODIS NDVI within GEE to disentangle the roles of climate and anthropogenic activities [14]. A comparable approach using Sentinel-2 NDVI in GEE was applied to assess vegetation changes in Al Jazirah, Sudan, linking shifts to environmental and socio-political factors [15]. Despite these advances, few studies have applied such integrated and data-driven approaches to arid river-dependent regions like southern Iraq. In particular, the relative influence of managed water resources (streamflow) compared to climatic factors on vegetation health has not been quantitatively evaluated across different land cover types in Thi-Qar Governorate. For example, [16] investigated precipitation and temperature impacts on the NDVI but did not incorporate local streamflow dynamics or assess their role relative to climate in a spatially explicit manner for this vulnerable governorate. In contrast, our current study uses satellite-derived agricultural and water productivity data from the FAO WaPOR (Water Productivity through Open access of Remotely sensed derived data) database to support a more process-based assessment of land degradation in Thi-Qar. WaPOR provides spatially consistent estimates of key variables, particularly net primary production (NPP) and actual evapotranspiration (ET), which help link vegetation conditions directly to water use and management. By combining WaPOR NPP with traditional vegetation indices such as the NDVI, this approach moves beyond monitoring vegetation cover alone and enables improved assessment of changes in carbon uptake and water productivity. This integrated framework aims to offer clearer insight into the interactions between human activities, water availability, and vegetation dynamics in these arid and semi-arid regions.

Recent research shows that vegetation dynamics in arid and semi-arid regions are shaped by the combined influence of climate variability and human activities such as land-use change, water use, and ecological restoration [17–19]. For example, recent studies have quantified how precipitation, temperature, and human impacts contribute to NDVI changes over long periods in river basins and other dryland landscapes and have separated the relative contributions of climatic drivers versus human activities [17,18]. These studies highlight that spatial heterogeneity and lagged responses are common in vegetation–climate interactions, especially in areas where human-managed water availability interacts with natural climate variability to control vegetation growth patterns [19].

According to the United Nations Development Business (UNDB), the region of Thi-Qar requires urgent attention for land rehabilitation [20]. Despite reported environmental deterioration in Thi-Qar [21], there has not yet been research to examine the spatiotemporal trend in vegetation and its relationship with climatic factors. Previous studies have often focused on isolated aspects of environmental degradation and have not leveraged remote sensing techniques and statistical models. Moreover, while some research has examined the impact of the NDVI on river flow in other regions, e.g., [22,23], no studies in Iraq have examined the impact of changing streamflow on vegetation nor established the relationship between precipitation and vegetation change across relevant land cover types. While many studies have focused on the northern parts of Iraq, the central and southern regions of the country require in-depth investigation to manage water resources and develop mitigation methods [24]. Iraq's water supplies are being impacted by climate change in several ways,

including decreasing river discharge, decreased rainfall and groundwater recharge, and loss of vegetation cover [24].

Based on the identified research gaps and the increasing environmental pressure in southern Iraq, this study focuses on Thi-Qar Governorate, a highly vulnerable arid region where vegetation dynamics are strongly dependent on river flow and managed irrigation. Declining streamflow, rising temperatures, and increasing water scarcity pose significant challenges to vegetation sustainability, yet the relative influence of hydrological and climatic drivers remains poorly quantified across different land cover types.

Accordingly, this study is guided by the following hypotheses:

(1) Vegetation dynamics in Thi-Qar are governed by the interaction between hydrological changes (streamflow) and climatic factors (precipitation, temperature).
(2) Areas with consistent water availability—whether from river flow or managed irrigation—will exhibit stable or improving vegetation trends, whereas water-scarce areas will show degradation, especially under rising temperatures.

The research questions this study aims to address are:

What are the spatiotemporal trends in vegetation represented by the NDVI across Thi-Qar Governorate over the past two decades?
What is the impact of streamflow and precipitation change on the different vegetation and non-vegetation classes?

We perform a spatiotemporal analysis of NDVI trends in the southern Iraqi region of Thi-Qar from 2001 to 2022 using MODIS data processed within the Google Earth Engine platform. The objectives are as follows: (1) to map pixel-based NDVI trends using the Mann–Kendall test and linear regression to identify areas of significant vegetation increase or decline; (2) to quantify rates of vegetation change across the region and link them to periods of climatic or anthropogenic influence; (3) to evaluate the relative impact of streamflow, precipitation, and land surface temperature on the NDVI through single and multiple regression models; (4) to compare NDVI–precipitation relationships between irrigated croplands and non-irrigated land classes to assess the role of water management; (5) to integrate WaPOR net primary production (NPP) data to validate vegetation productivity trends and support the NDVI-based findings.

2. Materials and Methods

2.1. Materials

2.1.1. Study Area

Thi-Qar Governorate, located in southern Iraq (Figure 1), covers about 13,841.65 km^2. It borders Wasit to the north, Basra to the south and southeast, Maysan to the east, Muthanna to the west, and Qadissiya to the northwest. Thi-Qar has an arid climate with hot summers and mild winters [21,25]. Temperatures can reach 51 °C (123 °F) in July and August and drop to zero in January. Rainfall, mostly occurring between December and April, averages 100–180 mm annually [26]. The main freshwater sources are the Euphrates River and the Al-Gharraf Stream (a Tigris River branch), which supply water to cities and marshes.

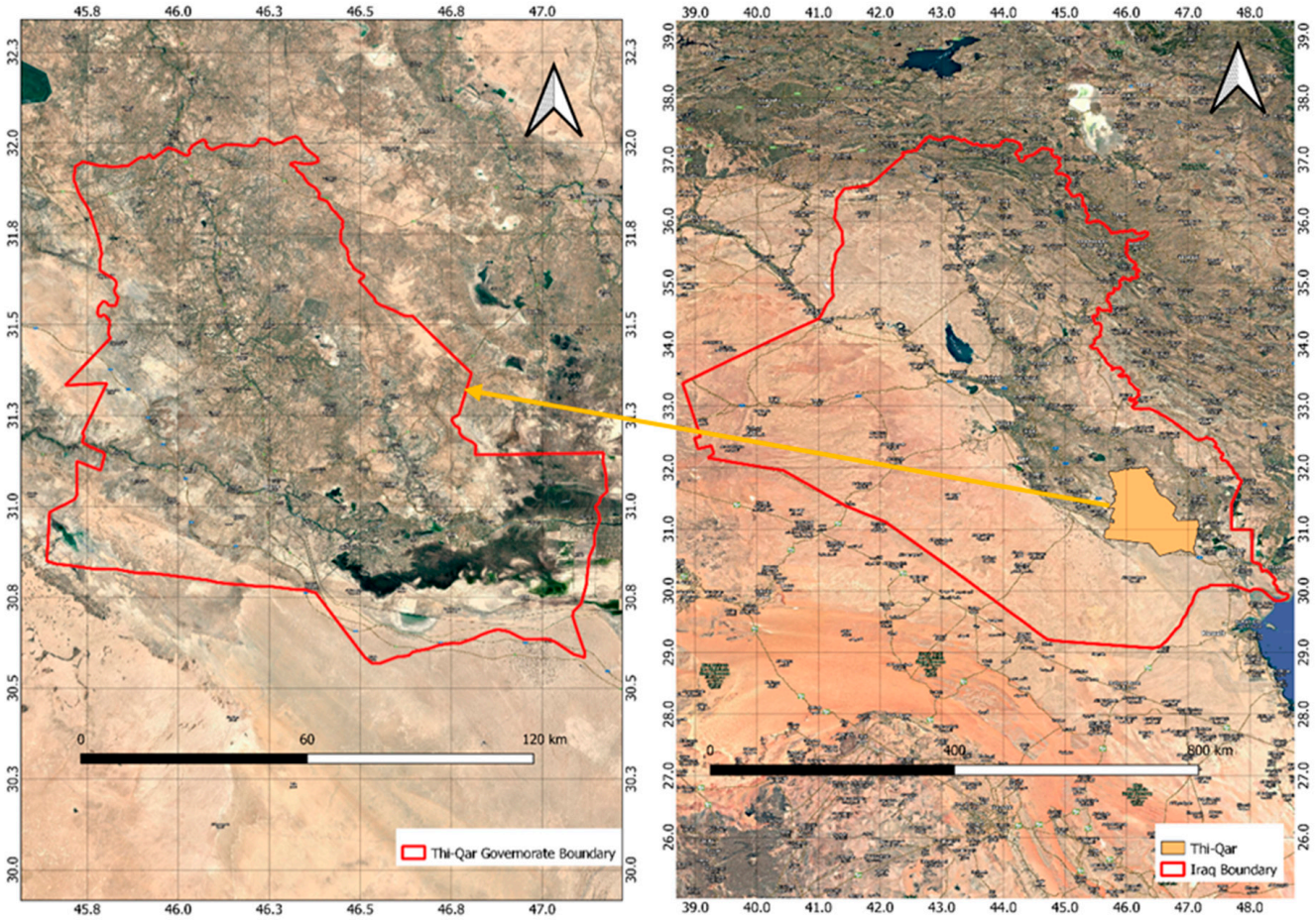

Figure 1. The study area location map.

2.1.2. Data Sources

Moderate-Resolution Imaging Spectroradiometer (MODIS) Satellite Data

Google Earth Engine (GEE) was utilized to process and analyze Moderate-Resolution Imaging Spectroradiometer (MODIS) Terra satellite vegetation index products (MODIS/061/MOD13Q1) from NASA [27], with a spatial resolution of 250 m. The NDVI equation is as follows:

$$\text{NDVI} = \frac{NIR - Red}{NIR + Red} \quad (1)$$

MODIS imagery was chosen for its high temporal resolution, consistent image availability, minimal cloud interference, and strong correlation with vegetation changes [28]. The MOD13Q1 product provides 16-day maximum value composites of atmospherically corrected surface reflectance, filtered for clouds, aerosols, and low-quality pixels [27]. The MODIS data were processed, filtered, and clipped using GEE to focus on the study area.

Satellite-Based Rainfall Data

A quasi-global rainfall dataset spanning more than 30 years is available from Climate Hazards Group InfraRed Precipitation with Station data (CHIRPS). For trend analysis and seasonal drought monitoring, CHIRPS creates gridded rainfall time series using in situ station data and satellite imagery with a resolution of 0.05° [29]. CHIRPS data have been widely applied in hydroclimatic studies, including recent work by [30]. Using GEE, we computed the daily precipitation. Then, we calculated the average monthly amount for the years 2001 through 2022.

WAPOR Dekadal Net Primary Production 2.0

Net primary production (NPP) represents the process by which photosynthesis converts carbon dioxide into biomass. In the WaPOR database, each pixel value represents daily NPP expressed as $g/m^2/day$ [31]. WaPOR (Water Productivity through Open access Remotely sensed derived data), developed by the Food and Agriculture Organization (FAO), provides data at three spatial resolutions (30 m, 100 m, and 250 m) covering different regions for the period 1 January 2009 to 3 January 2023 [31]. It has been widely used in related research, e.g., [32–34]. In our study, we use NPP at a 100 m spatial resolution level from 1 January 2009 to 31 December 2022.

Evapotranspiration

Evapotranspiration (ET) is an important process in the hydrological cycle, representing the sum of water evaporation from land surfaces and plant transpiration, and it measures kg/mˆ2/8 day [35]. MOD16A2 provides 8-day composite ET values at 500 m resolution, where each pixel represents the total ET accumulated over 8 days. The MODIS (Moderate-Resolution Imaging Spectroradiometer) provides a satellite-based method for estimating ET through a dataset known as MOD16. This dataset utilizes the Penman–Monteith equation adapted for remote sensing applications [36]. The MOD16 ET algorithm calculates daily ET by considering factors such as net radiation, air temperature, the vapor pressure deficit, surface resistance, and aerodynamic resistance, thereby integrating various climatic and biophysical inputs. The algorithm splits ET into daytime and nighttime components, accounting for different conditions during these periods. The MOD16 product offers global coverage at a spatial resolution of 500 m, with data from 2001 to the present [37]. In this work, we extracted evapotranspiration for the study region from 2001 to 2022 using the MOD16A2 ET product, which offers 8-day composite ET data using the GEE platform.

Streamflow Data

Streamflow data were obtained from the Iraqi Ministry of Water Resources for the period 2006–2022 (unpublished data). Measurements were collected from six gauging stations (regulators) located along the Al-Garaf River, a branch of the Tigris River. Each station was equipped with instruments for monitoring river discharge, providing daily records expressed in $m^3\ s^{-1}$. The Ministry routinely operates and maintains these stations for water resource management, ensuring measurement and quality control before providing the data.

Land Surface Temperature (LST)

Land surface temperature (LST) and emissivity readings are provided daily in a 1200 km × 1200 km grid by the MOD11A1 V6.1 product [38], from which we used the daytime land surface temperature. Satellite data is used here to capture the continuous spatial distribution features of the land surface; ground-based LST is limited due to the small number of ground stations and their discrete spatial distribution [39]. We computed the average monthly LST from daily MOD11A1 V6.1 using GEE for 22 years.

2.2. Methods

2.2.1. Mann–Kendall

The Mann–Kendall test [40,41] has been widely used to measure the trend in time series extracted from remote sensing [42–45]. It is a non-parametric measurement method to detect spatial and temporal trends and is robust to data distribution characteristics. Following the Earth Engine procedures, this approach detects monotonic trends in non-

seasonal or aggregated datasets such as the annual mean NDVI. Because the NDVI values used here represent annual means (2001–2022), serial dependence and seasonality are not significant, making the standard Mann–Kendall test suitable without additional pre-whitening. Here, we use it to examine the trend across the study area on a per-pixel basis.

Three classifications were identified from the slopes: increasing, no change, and decreasing. The following equations define the Mann–Kendall test [46,47]:

$$S = \sum_{k=1}^{n-1} \sum_{j=k+1}^{n} sgn(x_j - x_k) \quad (2)$$

where

$$Sgn(x_j - x_k) = \begin{cases} 1 & if\ x_j - x_k > 0 \\ 0 & if\ x_j - x_k = 0 \\ -1 & if\ x_j - x_k < 0 \end{cases} \quad (3)$$

The symbol S gives the value of the MK test, while x_j and x_k are the sequential values; n is the length of the data series. The variance in S and the standardized Z-test statistic are given by the following equation:

$$\mathrm{VAR(s)} = \frac{\mathrm{n}\ (n-1)(2n+5) - \sum_{i=1}^{m} t_i(t_i-1)(2t_i+5)}{18} \quad (4)$$

$$Z = \begin{cases} \frac{S-1}{\sqrt{VAR(S)}} & S > 0 \\ 0 & S = 0 \\ \frac{S+1}{\sqrt{VAR(S)}} & S < 0 \end{cases} \quad (5)$$

where n is the number of data points, m is the number of tied groups, and the Z statistic fits the standard normal distribution. A positive value for Z means there is a change with an upward trend, while a negative value means there is a decreasing or declining trend [48].

2.2.2. NDVI Linear Fit

Linear regression is a statistical technique that models the relationship between dependent and independent variables with a linear approach and is widely used in NDVI interpretation, e.g., [49–51]. Linear regression was used to compute the slope of the NDVI change and map its spatial distribution, providing quantification of the rate and direction of the NDVI change for each pixel in the study area.

To determine the long-term trends in vegetation, a linear fit was calculated for the NDVI time series at each pixel using the ee.Reducer.linearFit() function within GEE. This function computes the slope and intercept of the best-fit line for the NDVI values over 22 years. The slope, representing the rate of change in the NDVI, indicates whether vegetation is increasing or decreasing.

The equation used for the linear fit computation is as follows:

$$NDVI_{linear\ fit} = (Slope \times time) + Intercept \quad (6)$$

We classified the slope values relative to the standard deviation (σ) of the slope distribution. Five categories were defined: strongly decreasing ($\leq -1.5\sigma$), moderately decreasing (-1.5σ to -0.75σ), stable (-0.25σ to $+0.25\sigma$), moderately increasing ($+0.25\sigma$ to $+0.75\sigma$), and strongly increasing ($\geq +1.5\sigma$). The value of 1 sigma corresponds to an NDVI change of 0.0035/year). The σ-based classification was not used to establish any statistical relationship between the NDVI slope and its variability. Instead, it was applied to define and show how NDVI values change across the study area relative to the overall

scene variability. The mean and standard deviation of the NDVI slope were calculated from the regression results and used as thresholds to group the slope values into relative categories (e.g., strongly decreasing to strongly increasing). This method provides a clear, comparable representation of NDVI change intensity, consistent with previous NDVI trend analyses [52,53].

2.2.3. Land Cover Classification and Grouping into Vegetated and Non-Vegetated Classes

We classified the study area using Sentinel-2 imagery (COPERNICUS/S2_SR_HARMONIZED) and GEE, as shown in Figure 2, into eleven classes. We used supervised classification and the SmileCART algorithm. These classes are as follows: aquatic vegetation, arable land, bare areas, irrigated cropland, marshland, sandy areas and dunes, salted land, urban and industrial areas, water bodies, water courses, and wetland. From the eleven classes, we created four categories: one vegetated class (irrigated cropland) and three non-vegetated classes (arable land, bare areas, and sand areas and dunes) (Figure 3).

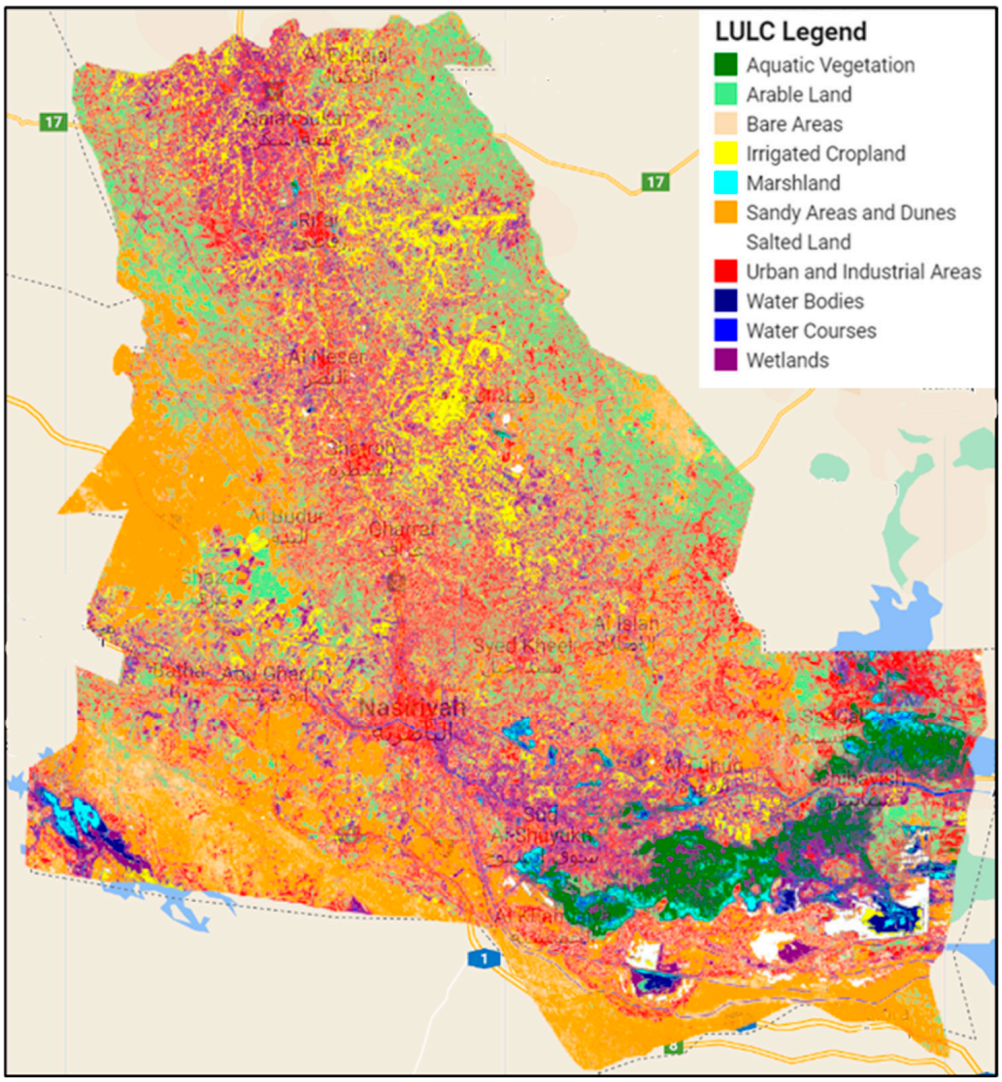

Figure 2. Land use land cover classification (LULC) for Thi-Qar Governorate from Sentinel-2 satellite data.

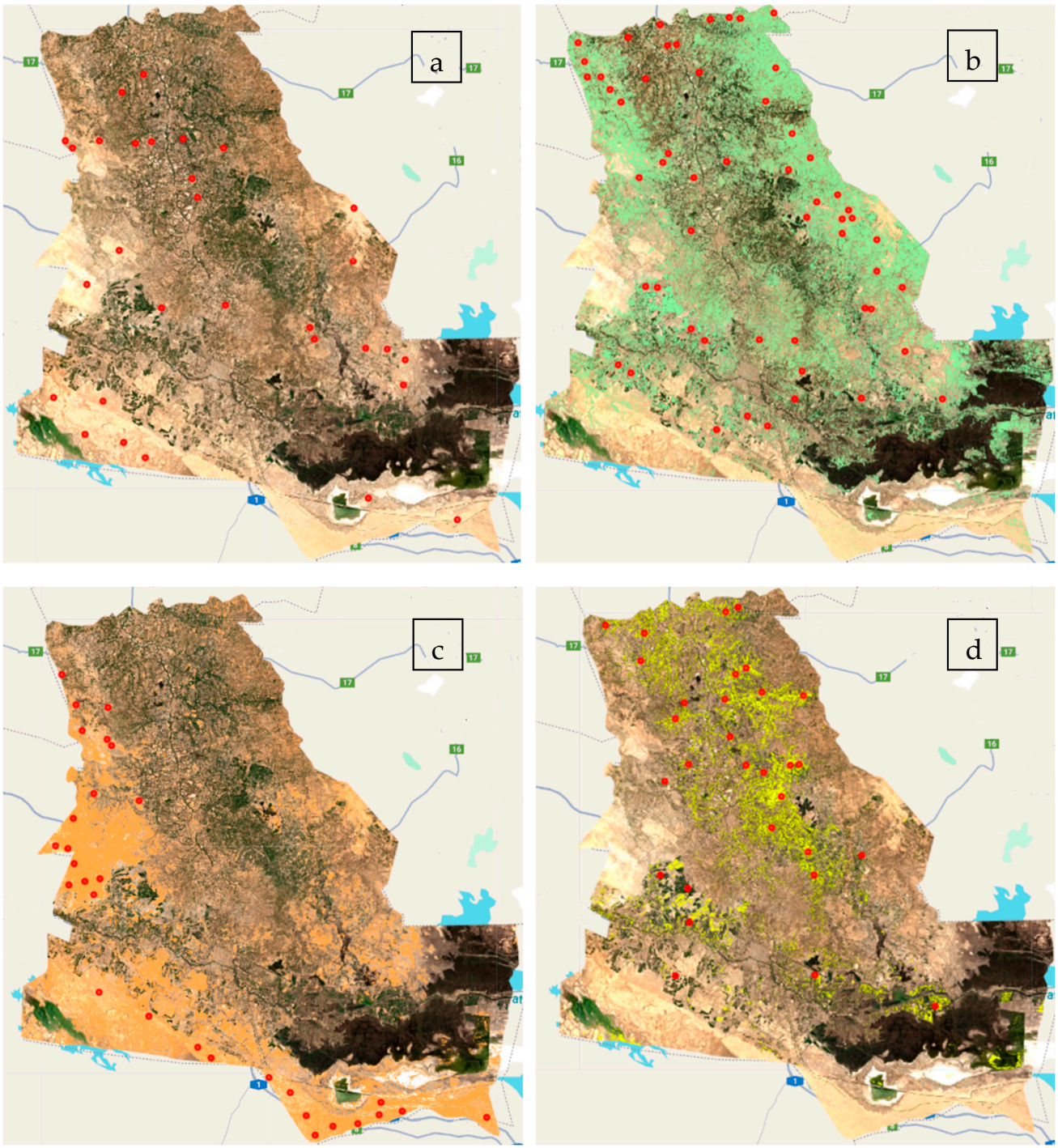

Figure 3. Spatial distribution of sample locations within land cover classes that were taken from the LULC map of the study area; red points indicate sample locations within each class. (**a**) Bare areas are represented in peach. (**b**) Arable land is represented in light green. (**c**) Sand areas and dunes are represented in orange. (**d**) Irrigated cropland is represented in yellow.

Within each of the four classes, we randomly selected representative samples (250 m × 250 m). Thirty samples were taken for cropland, bare areas, and sand areas and dunes and 55 samples for arable land. For each sample, the NDVI was computed for the 22 years using MODIS in GEE. This approach assumes that the land cover class for each pixel was consistent over the 22-year study period when extracting the NDVI time series. While this provides a clear framework for analyzing climate–vegetation relationships

within defined land types, it does not account for pixels that may have changed category (e.g., from cropland to bare area) during the analysis period.

2.2.4. Single and Multiple Regression Models

We applied both simple linear regression and multiple linear regression to evaluate the influence of climatic and hydrological variables on the NDVI.

Simple linear regression (6) was used to examine the individual relationship between the NDVI and each predictor variable (precipitation, land surface temperature, and streamflow). In addition, we applied the Spearman rank correlation coefficient (ρ) [54] to evaluate the strength and direction of monotonic relationships between the NDVI and the climatic/hydrological variables. The Spearman method is a non-parametric statistical measure that does not assume linearity or normal distribution of data and is less sensitive to outliers, making it suitable for detecting both linear and nonlinear monotonic associations.

A multiple regression model was used to evaluate the combined effect of multiple factors. The model is expressed as follows:

$$NDVI_{linear\ fit} = a_1.\ Precipitation + a_2.\ LST + a_3.\ Streamflow + Intercept \quad (7)$$

where

a_1, a_2, and a_3 are the regression coefficients showing the contribution of each factor.
In addition to multiple regression, partial correlation analysis [55,56] was employed to quantify the unique relationship between the NDVI and each predictor variable while controlling for the others. The first-order partial correlation coefficient $P_{XY,Z}$ between variables X and Y, while controlling for a third variable Z, is calculated as follows [57,58]:

$$P_{XY,Z} \frac{P_{XY} - P_{XZ}P_{YZ}}{\sqrt{(1 - P^2{}_{XZ}).(1 - P^2{}_{YZ})}} \quad (8)$$

- P_{XY} = Correlation between variable X and Y
- P_{XZ} = Correlation of the third variable Z with the variable X
- P_{YZ} = Correlation of the third variable Z with the variable Y

2.2.5. Data Harmonization

All raster datasets were harmonized to a consistent 250 m spatial resolution before statistical analysis to ensure pixel-to-pixel comparability. This was accomplished within Google Earth Engine by specifying a target scale of 250 m and applying the ee.Reducer.mean() reducer during all overlay and extraction operations. For coarser-resolution datasets (e.g., CHIRPS precipitation at ~5.5 km, MODIS LST at 1000 m), this process effectively downscaled values to the 250 m grid using spatial interpolation. For finer-resolution data (e.g., WaPOR NPP at 100 m), values were aggregated to the 250 m grid by averaging. This approach ensures that every pixel in the final analysis stack represents the same ground area (250 m × 250 m), eliminating scale mismatch as a source of bias in correlation and regression models.

3. Results

We applied the Mann–Kendall trend test to the NDVI data for Thi-Qar Province to evaluate spatial–temporal changes in vegetation cover for the period from 2001 to 2022. The results are visualized in Figure 4, which shows areas of increasing and decreasing NDVI trends. The value of the trend is between −1 and 1, which represents the strength of the NDVI direction over 22 years. The analysis showed spatial patterns in vegetation change: areas shown in green on the map indicate regions with a positive trend in the NDVI,

suggesting the majority of years showed an increase in vegetation cover over the study period. These areas are in the central, northern, and southern parts of the Thi-Qar region. Regions in red represent areas with a negative NDVI trend, which is a decline in vegetation cover for the majority of years. These trends are in the southern and southeastern parts of the region. Areas with no trend are off-white, indicating stable vegetation cover.

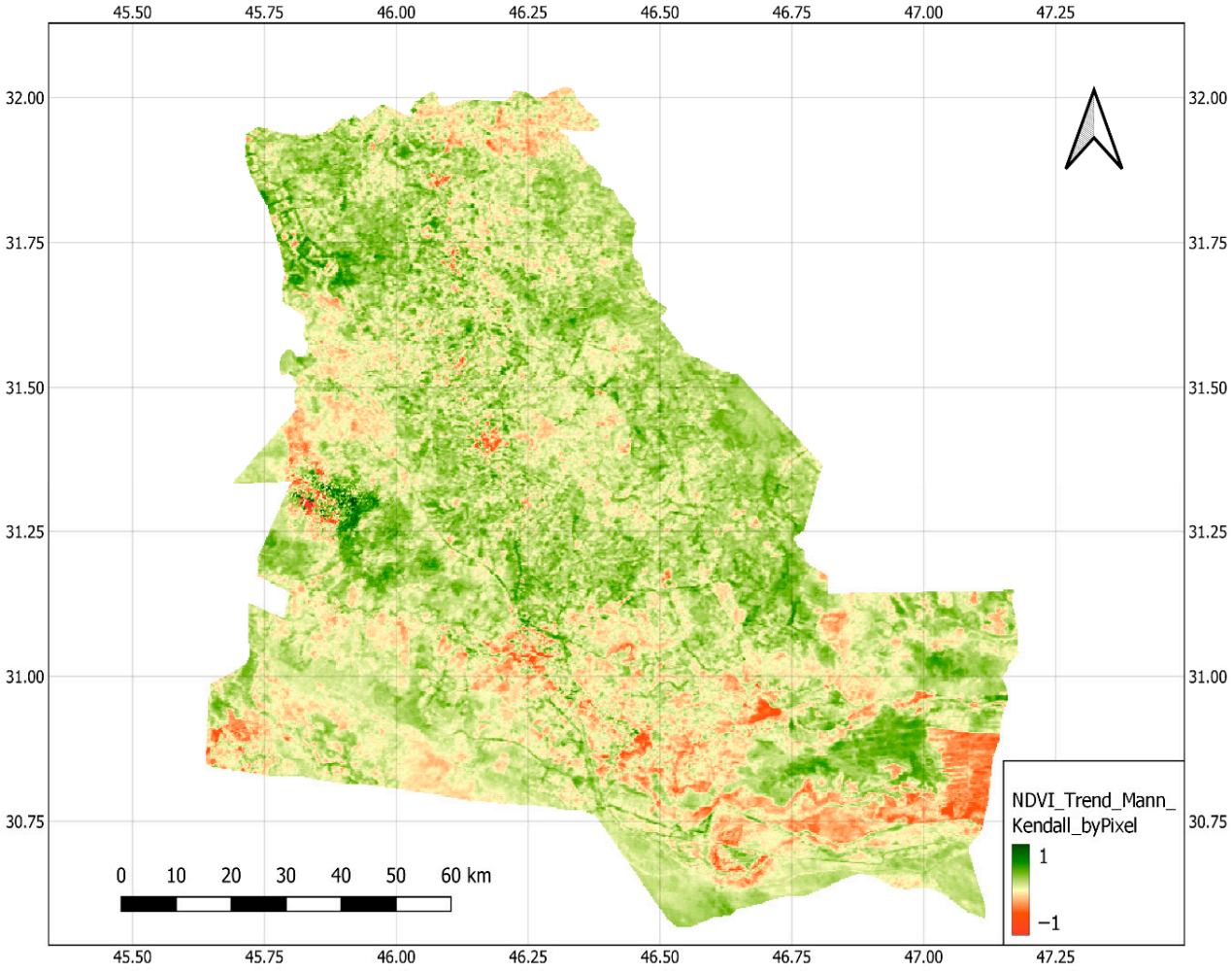

Figure 4. Spatiotemporal NDVI trend for Thi-Qar over 22 years using the Mann–Kendall test. Green regions indicate an increasing NDVI trend, off-white regions indicate no trend, and red regions indicate a decreasing NDVI trend.

Quantification of the rate of change in the NDVI at each pixel was determined by applying linear regression, as shown in Figure 5. The resulting slopes show vegetation trends throughout the study area. The color ranges from red, showing a strongly decreasing NDVI, to dark green, corresponding to a strongly increasing NDVI. The classification of trends showed that 27.16% of the area was strongly decreasing, 29.32% was moderately decreasing, 31.46% was stable, 7.57% was moderately increasing, and 4.49% was strongly increasing. This means that a large area of Thi-Qar presented declining or stable vegetation productivity, with only ~12% showing a positive trend.

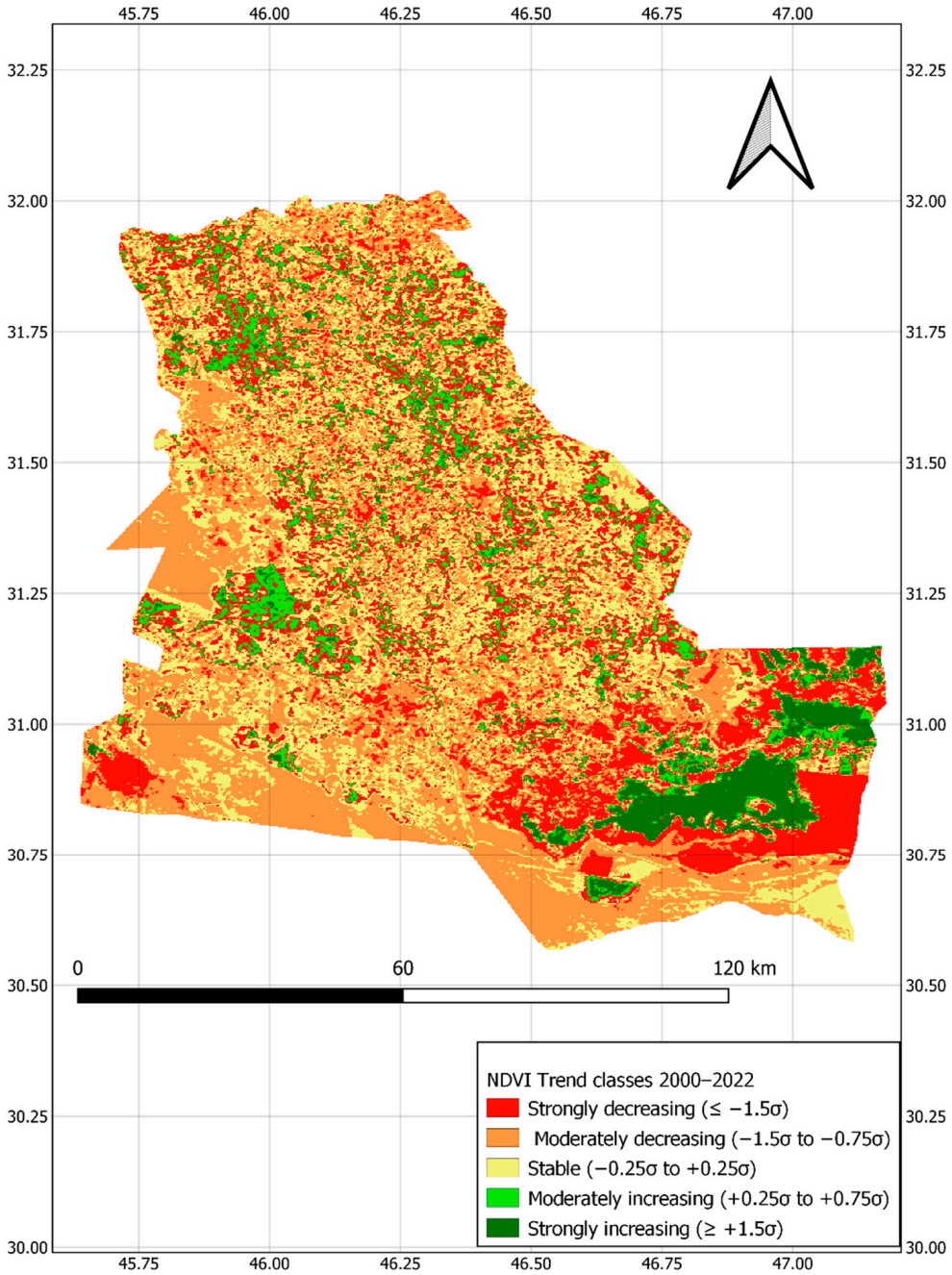

Figure 5. Spatial distribution of NDVI linear trends in Thi-Qar Province from 2001 to 2022, derived from MODIS MOD13Q1 (16-day composites). Linear regression slopes of the NDVI time series were classified relative to the standard deviation (σ) of slope values. Five trend categories are shown: red to orange are decreasing vegetation productivity, yellow is stable, light to dark green is increasing trends.

The time series analysis of the annual NDVI for Thi-Qar Governorate over 22 years is shown in Figure 6. There was a fluctuation in vegetation cover during this period. The graph indicates a generally increasing trend in the NDVI, with a calculated linear regression slope of about 0.0019. The R value of 0.47 reflects the relationship between time and the NDVI ($p < 0.05$), where y represents the NDVI and x represents time in years. Despite variations in some years, there is a slight upward trend in the NDVI, as shown in Figure 6.

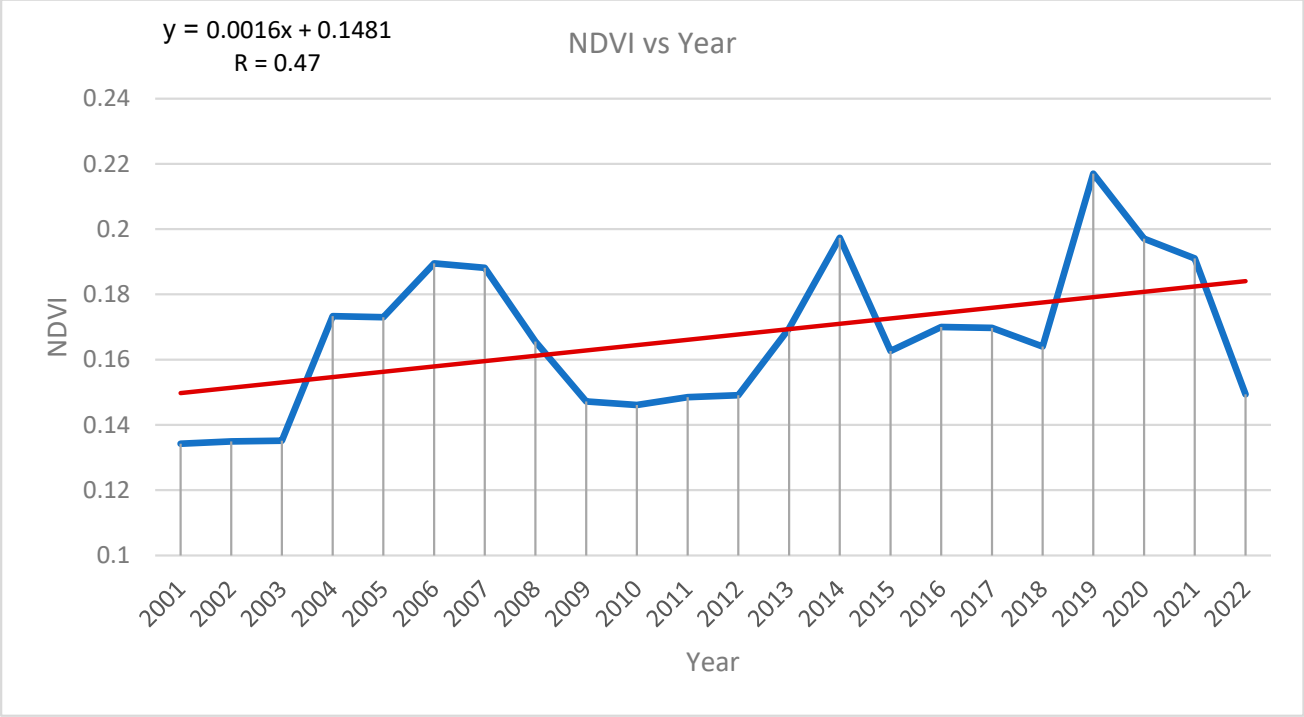

Figure 6. Time series of the annual averaged NDVI in Thi-Qar. The line represents the linear fit of the NDVI over the time series from 2001 to 2022.

To understand the reasons for regions of degradation and vegetation increase and their impacts, we examined the relationship between the NDVI and climatic and hydrological factors, with correlations shown in Figures 7–10. Both Pearson's linear correlation and Spearman's rank correlation were used to assess the strength and significance of these relationships. The NDVI showed a positive correlation with precipitation ($R = 0.40$; $\rho = 0.43$, $p < 0.001$) (Figure 7a–c). In contrast, it showed a negative correlation with land surface temperature ($R = -0.50$, $\rho = -0.46$, $p = 0.027$) (Figure 8a,b). As expected, the NDVI was strongly positively correlated with evapotranspiration ($R = 0.74$, $\rho = 0.72$, $p < 0.001$) (Figure 8c,d) and with net primary production ($R = 0.95$, $\rho = 0.93$, $p < 0.0001$) (Figure 8e,f). Finally, the NDVI also correlated positively with the monthly ($R = 0.51$, $\rho = 0.51$, $p < 0.001$) (Figure 9a,b) and annual ($R = 0.8$, $\rho = 0.78$, $p < 0.001$) (Figure 10) streamflow.

Secondly, to understand the independent influence of each environmental factor on the NDVI, we calculated partial correlation coefficients, which measure the correlation between two variables while statistically controlling for the effects of others. This approach helps reduce confounding and provides a clearer picture of each driver's contribution. The results (Table 1) show that streamflow has the strongest association with the NDVI ($\rho = 0.53$), followed by LST ($\rho = -0.47$) and precipitation ($\rho = 0.46$). All partial correlations were statistically significant ($p < 0.001$).

Table 1. Comparison of simple and partial correlation coefficients.

Relationship	Controlling For	Partial Correlation (ρ)
Streamflow vs. NDVI	Precipitation & LST	0.53
Precipitation vs. NDVI	Streamflow & LST	0.46
LST vs. NDVI	Streamflow & Precipitation	−0.47

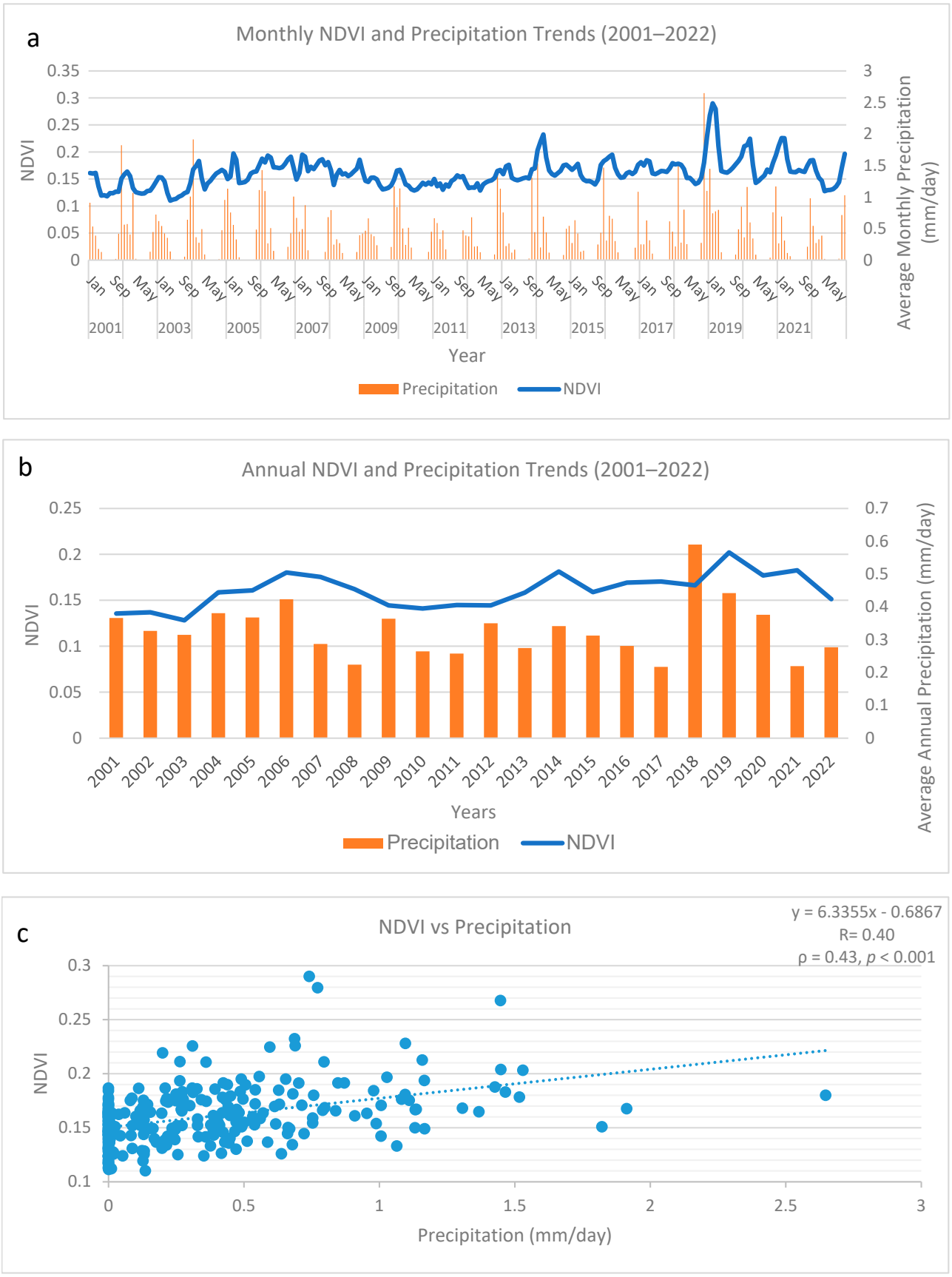

Figure 7. (**a**,**b**) Monthly and annual trends for the NDVI and precipitation (2001–2022). (**c**) Relationship between the NDVI and precipitation.

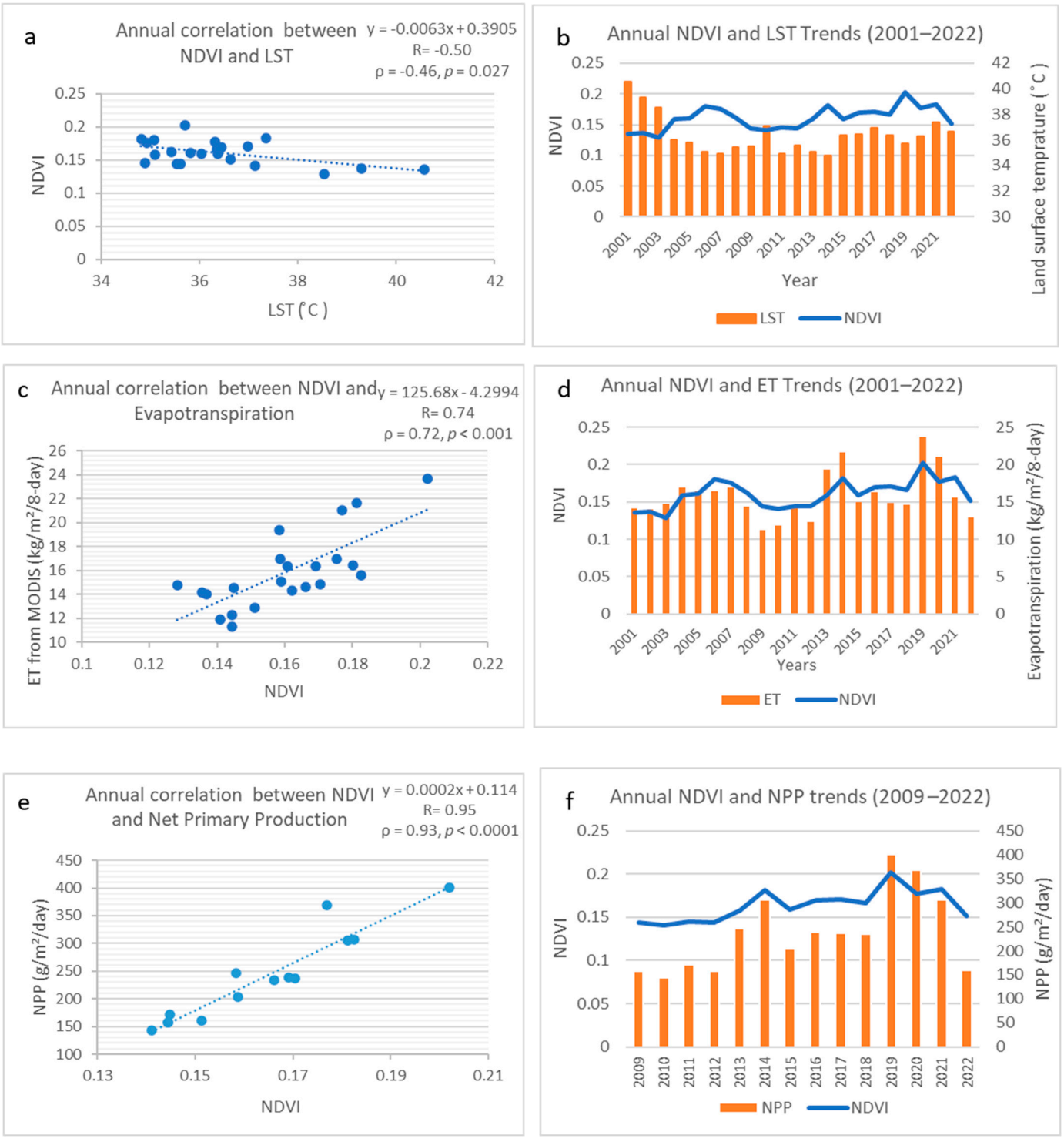

Figure 8. (**a**,**c**,**e**) The correlation between the NDVI and LST, ET, and NPP. (**b**,**d**,**f**) The annual variation in the NDVI and LST, ET, and NPP.

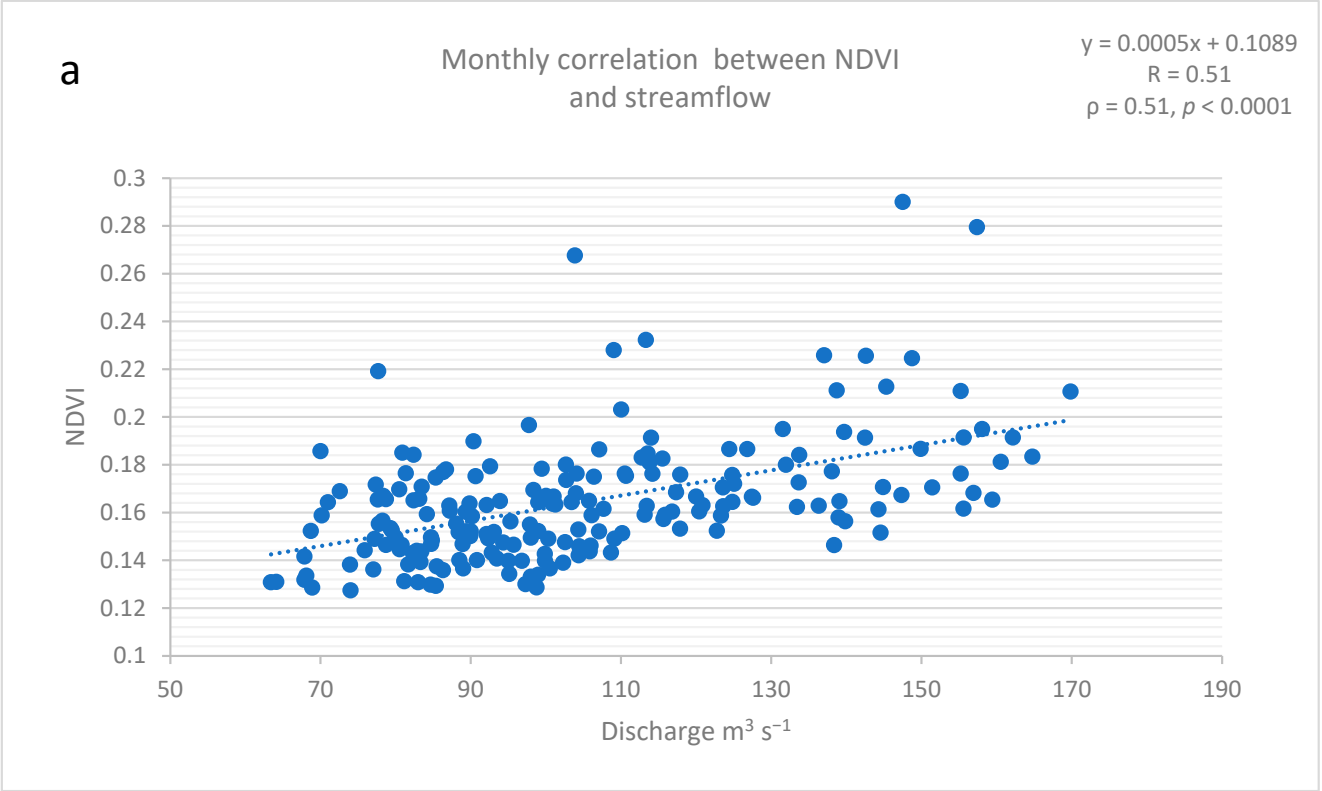

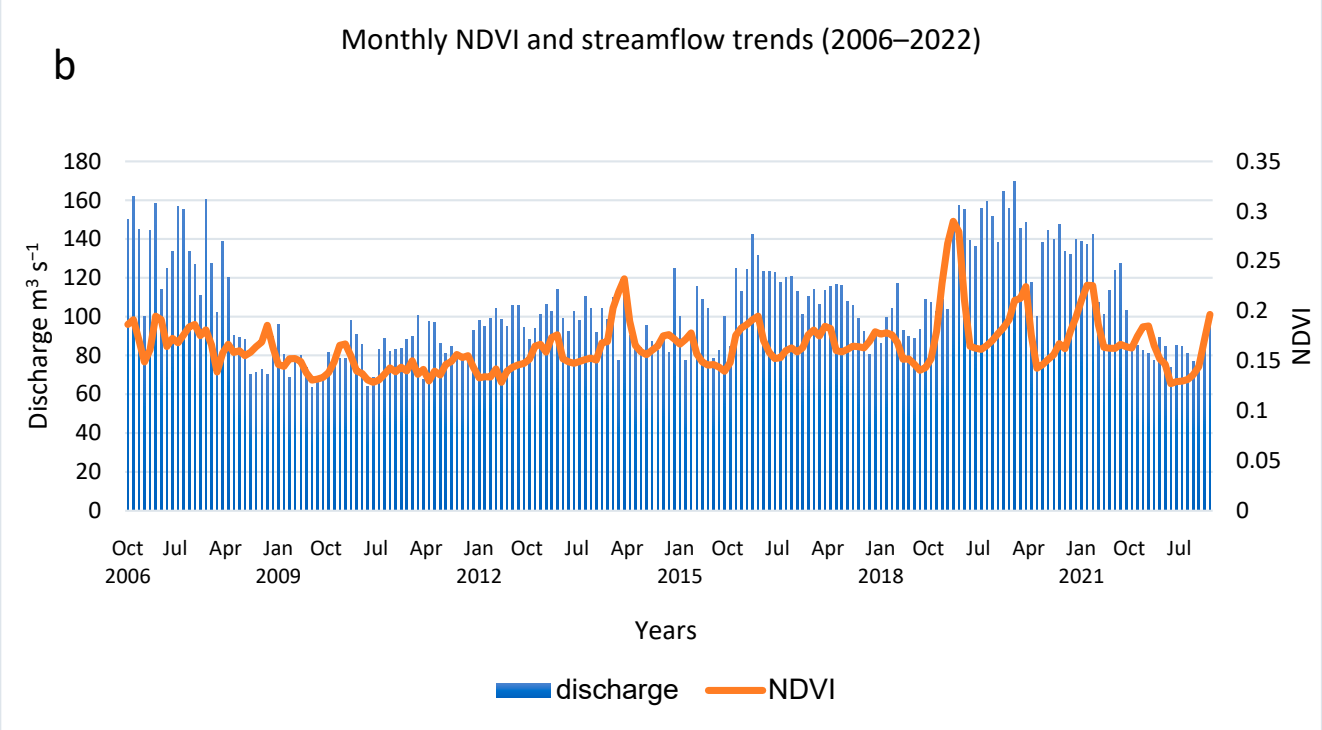

Figure 9. (**a**) The correlation between streamflow and the NDVI. (**b**) The monthly variation in the NDVI and streamflow over the years.

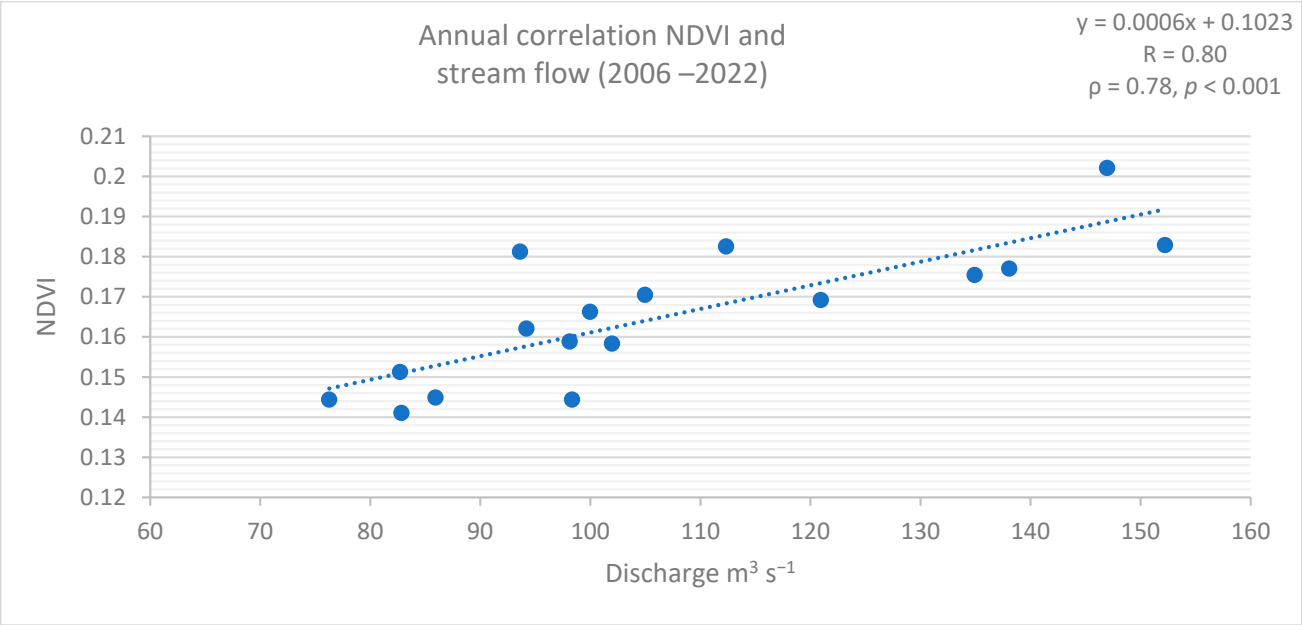

Figure 10. The annual relationship between the discharge of streamflow and the NDVI.

The monthly and annual relationship between river flow and both vegetation (irrigated croplands) and non-vegetation land types (arable land, barren areas, and sand dunes) were found for 2006 to 2022, as shown in Table 2. The relationships between streamflow, precipitation, and the NDVI for the four land cover classes are presented in Tables 2–4. For each linear regression (NDVI = a × Predictor + b), 'a' represents the slope (rate of change in the NDVI per unit change in the predictor), 'b' is the intercept, and 'R' is the Pearson correlation coefficient.

Table 2. The monthly and annual relationship between the discharge of streamflow and the NDVI for the vegetation and non-vegetation classes: (A) irrigated cropland, (B) bare areas, (C) arable lands, and (D) sand area and dunes.

Monthly correlation between streamflow and NDVI for vegetation and non-vegetation classes (2006–2022)				
Class	Land Cover Type	a	b	R
A	Cropland class	0.0009	0.1597	0.21
B	Bare area class	0.0003	0.0782	0.26
C	Arable land	0.0007	0.0777	0.41
D	Sand & dunes areas	0.0002	0.064	0.26
Annual correlation between streamflow and NDVI for vegetation and non-vegetation classes (2006–2022)				
Class	Land Cover Type	a	b	R
A	Cropland class	0.0008	0.1703	0.55
B	Bare area class	0.0002	0.0814	0.37
C	Arable land	0.0005	0.107	0.46
D	Sand & dunes areas	0.0002	0.0608	0.49

Table 3 shows the relationship between 1-month-lagged monthly precipitation and the NDVI for the vegetation and non-vegetation classes. According to earlier studies, we may expect a lag in the monthly NDVI response to rainfall [59]. We found that there is a stronger link between the monthly NDVI and the monthly precipitation from the previous month than there is with the monthly precipitation from the same month. While Table 3 demonstrates a moderate-to-strong monthly relationship (with a 1-month lag), Table 4

shows a weaker annual correlation between precipitation and the NDVI across all classes. Notably, the correlation coefficient (R) decreases substantially for the cropland and arable land vegetation classes.

Table 3. The monthly relationship between precipitation and the NDVI for the vegetation and non-vegetation classes (with a 1-month lag).

Monthly correlation between precipitation and NDVI for vegetation and non-vegetation classes (2001–2022)				
Class	Land Cover Type	a	b	R
A	Cropland class	0.1419	0.1999	0.62
B	Bare area class	0.0324	0.0931	0.56
C	Arable land	0.0583	0.1326	0.55
D	Sand & dunes areas	0.0157	0.0745	0.47

Table 4. The annual correlation between precipitation and the NDVI for the vegetation and non-vegetation classes: (A) irrigated cropland, (B) bare areas, (C) arable lands, and (D) sand area and dunes.

Annual correlation between precipitation and NDVI for vegetation and non-vegetation classes (2001–2022)				
Class	Land Cover Type	a	b	R
A	Cropland class	0.109	0.2104	0.30
B	Bare area class	0.0726	0.0808	0.37
C	Arable land	−0.0142	0.1566	−0.05
D	Sand & dunes areas	0.0547	0.0626	0.47

Finally, a multiple regression model was first applied between the NDVI and the factors (LST, streamflow, and precipitation) for the whole study area. It was then conducted separately for the vegetation and non-vegetation classes to estimate the impact of the factors on land cover types (Tables 4 and 5).

Table 5. Multiple regression model between streamflow, precipitation, LST, and the NDVI.

Multiple regression model						
Statistics Value						
Multiple R	0.671493					
R Square	0.450902					
Adjusted R Square	0.442232					
Standard Error	0.019255					
Observations	194					
ANOVA						
Source	df	SS	MS	F	Significance F	
Regression	3	0.057845	0.019282	52.00742	1.38×10^{-24}	
Residual	190	0.070442	0.000371			
Total	193	0.128288				
Variable	Coefficients	Standard Error	t Stat	*p*-value	Lower 95%	Upper 95%
Intercept	0.130711	0.009848	13.27317	7.07×10^{-29}	0.111286	0.150136
Discharge	0.000477	5.58×10^{-5}	8.549923	4.02×10^{-15}	0.000367	0.000587
Precipitation	0.013358	0.00511	2.61401	0.009666	0.003278	0.023438
LST	−0.00058	0.000181	−3.18234	0.001707	−0.00094	−0.00022

4. Discussion

Analysis of NDVI trends in Thi-Qar Governorate from 2001 to 2022, using the Mann–Kendall trend test and linear regression, provides important insights into changes in vegetation and potential land degradation processes.

4.1. Spatial Analysis of Vegetation Changes

The spatial patterns in vegetation change shown by the Mann–Kendall test confirm the critical role of water availability, with degradation concentrated in areas distant from perennial water sources, which are more apparent in the northwest and central regions. In the southeast, the pattern is more complex, with positive trends near the rivers and wetland but also in areas of degradation. This finding agrees with [60], who reported that vegetation cover remained relatively dense in river-fed and marsh areas. These insights suggest a need for large efforts in land restoration in areas with negative trends. While some areas do not show positive or negative trends, continued monitoring is necessary to ensure they do not move into declining trends. These findings highlight that streamflow plays a more important role than rainfall in determining vegetation dynamics in Thi-Qar. Marshes and croplands depend on river water, which can buffer against degradation, while rainfall is highly variable and often insufficient. Effective water management, including regulated discharge and irrigation practices, is therefore essential to maintain vegetation productivity.

Linear regression analysis of the NDVI data for vegetation cover in Figure 5 showed a clear variation in the study area. Here, degradation is apparent in the southern and western regions of the governorate, which are the marshes and dune areas, respectively. The result contrasts with the Mann–Kendall trend, which suggests that, despite the majority of years showing greening for much of the area, the net change over the period is a decline in productivity for the majority of the region. This can be explained by the impact of less frequent drought events outweighing gradual greening from climate trends. This decline is consistent with [61], who reported reduced vegetation in the same regions, attributed to recurrent drought events and declining precipitation. Previous research [59] also confirmed a long-term reduction in vegetation cover (~80% decline between 1990 and 2022) due to decreased Euphrates discharge, rising evaporation, and land degradation. In contrast, the northern parts of the marsh region showed a strong increase in the normalized difference vegetation index due to the constant presence of water in this area—an increase in reed and papyrus plants is clear from the LULC classification. Globally, linear regression in Google Earth Engine has been applied to map NDVI trends [62,63], and recent studies in Iraq have also utilized GEE for vegetation trend analysis [64,65]. However, to the best of our knowledge, no previous studies in Thi-Qar Governorate or in southern Iraq's riparian systems more broadly have applied this approach within an integrated multi-source framework that combines pixel-wise trend analysis with multi-factor regression using harmonized local streamflow data, WaPOR NPP, and climate variables to clearly partition the impact of hydrological management from climatic drivers across land cover classes.

4.2. Temporal Analysis of Vegetation Changes

The temporal variability in vegetation activity in Thi-Qar reflects the combined influence of hydrological management, climate variability, and delayed ecosystem responses. Periods of increased vegetation greenness correspond to phases of enhanced inundation and improved water availability, while extended declines align with regional drought events and reduced upstream discharge. The results showed peaks in 2006, 2014, and 2019, followed by a sharp decline in 2022. This study agrees with [66], who reported that the Iraqi Center for Marsh Restoration developed a plan for restoration from 2009 to 2020 based on available data. They reported that the highest restoration rate occurred in 2014 but

lasted only for that year, then declined before increasing again in 2018, and that vegetation cover peaked in 2018, likely due to stable inundation rates from 2014 to 2018 compared to earlier periods. However, our results show that the NDVI increase peaked strongly in 2019, as shown in Figure 6. The one-year variance between the reported peak in vegetation restoration (2018) and the observed NDVI maximum (2019) may be explained by both spatial/ecological differences and lag effects in vegetation response. Additionally, increasing precipitation at the end of 2018, as shown in Figure 7a, further enhanced vegetation expansion in 2019. We also see a decline in the NDVI from 2007, which continued at a sustained low level for the period 2009–2012. A study reported a 2008–2009 drought in upstream countries like Turkey and Syria, along with reduced runoff from Iran, which may contribute to this change [67,68]. It is also important to consider human interventions in water management. Upstream water control, irrigation practices, and area restoration efforts can increase or decrease the effects of natural hydrological fluctuations. For instance, even years with higher rainfall may not show increases in the NDVI if water is diverted to agricultural use or lost due to inefficient irrigation.

Despite these fluctuations, the overall mean NDVI shows a slight increasing trend, which contrasts with the spatial linear regression results, where only 12% of the total area showed an increasing trend. This difference arises from the contribution of small regions of very strong positive change in the wetland area, which masks larger areas of moderate decline.

4.3. Impact of Individual Climate Drivers

The moderate correlation between the NDVI and precipitation (R = 0.40) suggests that rainfall alone is an insufficient driver of vegetation growth in Thi-Qar, a finding consistent with irrigated arid systems where human water management overrides climatic signals. This contrasts with many rain-fed dryland systems, where vegetation greenness is strongly coupled with precipitation variability [69–71]. In irrigated and river-fed landscapes such as southern Iraq, human-managed water resources override climatic signals, reducing the direct influence of rainfall on vegetation productivity. The relationship between land surface temperature (LST) and the NDVI was examined over 22 years. LST has a control on vegetation dynamics through its influence on evapotranspiration and soil moisture loss. The annual average temperature decreased from 41 °C in 2001 to 36 °C in 2006, corresponding with an increase in NDVI values of 0.13 in 2001 to 0.18 in 2006. Subsequently, the temperatures were almost stable at approximately 35 degrees Celsius, as shown in Figure 8b. Although [72] reported that temperatures are constantly increasing in Iraq, especially in its southern regions, our results indicate a different pattern in this study area.

Higher temperatures increase evapotranspiration rates, reducing soil moisture and negatively impacting vegetation productivity, particularly in arid regions [73]. However, the fluctuation in the NDVI was also caused by the additional factors of surface water, human interventions, and variation in rainfall. As [74] reported, human activities like land-use change, water mismanagement, and agricultural practices can interact with climatic stressors, accelerating ecosystem degradation and influencing vegetation dynamics. Negative correlation may, in part, also be explained by the fact that higher vegetation cover will result in surface cooling due to increased evapotranspiration, e.g., [75]. The partial correlation analysis confirmed the regression results, confirming that streamflow showed the strongest unique relationship with the NDVI (p = 0.53) when controlling for precipitation and temperature effects. This indicates that water resources are the most important factor in explaining vegetation dynamics in this arid region. The stronger correlation of the NDVI with streamflow compared to precipitation indicates that water availability from rivers is a determinant of vegetation dynamics in arid regions. Maintaining

streamflow ensures the stability of lands and supports crop growth, which has important ecological and socio-economic implications, including the preservation of biodiversity and agricultural productivity.

4.4. Implications of Multiple Regression Analysis

The multiple regression models confirm that streamflow is the dominant controllable factor influencing the NDVI, explaining why croplands near river channels showed resilience despite climatic variability. The model in Table 5 shows a moderate correlation coefficient (R = 0.67), with streamflow, precipitation, and LST influencing the dependent variable. Interestingly, streamflow has the strongest positive effect, followed by precipitation. LST shows a negative impact. LST represents a key climatic driver of water and heat stress in arid regions; however, a higher NDVI will also lead to surface cooling through transpiration. So, the negative coefficient for LST likely represents a combination of the stress imposed by high temperatures and the cooling effect of vegetation.

When we apply this regression to only areas classified as cropland, the correlation coefficient increases to R = 0.78, as shown in Table 6. Both streamflow and precipitation are crucial for maintaining cropland, as evidenced by their positive effects on the NDVI. This underscores the importance of sufficient water supply, whether through irrigation or rainfall, for crop productivity. The *p*-value shows that the LST has a greater impact than the discharge of streamflow and precipitation. These results are consistent with the study by [76], which confirmed the importance and positive impact of rainfall and river water on vegetation in addition to the negative impact of temperature on the NDVI.

Table 6. Multiple regression model between streamflow, precipitation, LST, and the NDVI separated into land cover types.

Land Cover Type	R	Adjusted R	Significance F	Streamflow Coefficient (*p*-Value)	Precipitation Coefficient (*p*-Value)	LST Coefficient (*p*-Value)
Cropland	0.78	0.77	1.11×10^{-37}	0.0005 (0.006)	0.042 (0.019)	−0.0057 (<0.001)
Bare Areas	0.26	0.23	0.004	0.0002 (0.004)	0.04 (0.019)	0.000409 (0.028)
Arable Lands	0.75	0.72	1.63×10^{-30}	0.0006 (<0.001)	0.02 (0.009)	−0.0018 (<0.001)
Sand Dunes	0.51	0.50	1.39×10^{-12}	0.0001 (0.002)	0.01 (<0.001)	−0.00013 (0.288)

For non-vegetation categories, correlations were weak for bare areas (Table 6) and dune areas, primarily due to limited vegetation. A lack of vegetation cover, combined with continuous exposure to high temperatures, leads to the loss of soil organic carbon. Even with increased rainfall or streamflow during specific periods, the potential for plant growth remains limited. Prolonged exposure of bare land and increased tillage have been shown to affect soil organic carbon [77], which impacts soil fertility and reduces vegetation growth. In contrast, the model for arable areas shows a strong correlation coefficient (R = 0.75), with positive effects from streamflow and precipitation and a negative impact from LST. Streamflow is the most influential factor here. Arable lands depend highly on water availability, with streamflow and precipitation playing crucial roles in supporting crop growth.

4.5. Limitations and the Role of Land-Use Change

This study focuses on the relationship between streamflow variability and the NDVI responses of dominant land cover types rather than on quantifying LULC transitions. Although land-use change driven by human activities can influence vegetation dynamics and hydrological processes, multi-temporal land-use change analysis was beyond the scope of this work. Future studies should integrate land-use change detection to better isolate the effects of anthropogenic activities on vegetation–hydrology interactions. Also, streamflow data were limited to 2006–2022 because of data availability. The MODIS NDVI product, while temporally consistent, has a 250 m resolution that may overlook fine-scale vegetation changes.

4.6. Importance of Streamflow to Vegetation Change

Iraq depends on the Euphrates and Tigris Rivers for most of its water demands [78]. More than 90% of all water withdrawals from Iraq are used for agriculture [79]. Rice, corn, dates, cotton, vegetables, fruits, and legumes are among the irrigated summer crops. Winter crops that are irrigated include barley and wheat. Most irrigation uses extremely inefficient techniques for food irrigation, resulting in water loss from unnecessary evaporation [80]. So, studying how surface water affects vegetation is important.

The analysis is illustrated in Figure 9a, which presents the relationship between stream discharge measured in cubic meters per second and the NDVI. The correlation coefficient R was 0.51 and the Spearman correlation was $\rho = 0.51$ ($p < 0.001$), suggesting that increased streamflow water availability strongly enhances vegetation productivity. Figure 9b shows the monthly trends in the NDVI and streamflow from 2006 to 2022. Throughout this period, fluctuations in streamflow appear to align with variations in the NDVI, further supporting the positive relationship observed in the scatter plot. Notably, the increases in runoff observed in 2016, 2019, and 2021 correspond to rises in vegetation productivity. Conversely, increases in stream discharge during other months of other years led to decreases in the NDVI, which may, in part, be explained by the fact that these months correspond to crop harvest season and that sometimes too much flow destroyed crops, especially next to rivers.

The correlation coefficient dramatically rose to 0.80 and the Spearman correlation to $\rho = 0.78$ ($p < 0.001$) when the yearly relationship was investigated (Figure 10). This rise implies a more robust streamflow–NDVI relationship for agriculture annually. Seasonal farming operations can account for the difference in correlations between the monthly and annual data. Increases in streamflow, for example, cannot immediately impact vegetation productivity during harvest seasons, resulting in reduced monthly relationships. Another factor for this variation is the increase in streamflow during times that farmers who did not prepare their land within the agricultural plan did not expect.

This finding is consistent with prior work [81] connecting hydrology and vegetation that examined the effect of NDVI trends and hydrological changes on vegetation dynamics in the Ejina Oasis in the lower reach of the Heihe River. It found that climate change influenced vegetation growth in the upper basin, while excessive water use caused degradation in the lower basin. The study effectively linked streamflow reduction and increased evapotranspiration to vegetation decline, highlighting the role of water resource allocation. These results confirm the importance of managing streamflow to optimize vegetation productivity. Proper scheduling of irrigation and controlled release from upstream reservoirs could enhance vegetation growth while minimizing crop losses during harvest or flood periods.

4.7. Implications for Management and Ecology of the Region

This study offers important insights into managing vegetation and water resources in Thi-Qar Province and similar arid regions. The importance of streamflow has been highlighted, and this variable can be controlled to an extent by water management. The impact on the NDVI has been highlighted, and this also leads to ecologically significant changes in productivity (NPP) and evapotranspiration (ET). From previous studies [82,83], we expect a strong correlation between the NDVI and both ET and NPP. Figure 8c shows the positive correlation between evapotranspiration (ET) and the normalized difference vegetation index (NDVI) observed in our study, with a correlation coefficient of 0.74. This relationship is clearly illustrated in Figure 8d, which shows parallel annual variations in the NDVI and ET. Specific years such as 2006, 2013, 2014, and 2019, with high ET values, correspond to strong vegetation growth and active transpiration. Conversely, the years with lower ET values (2008–2012, 2015–2018, and 2022), between 11 and 13 $kg/m^2/year$, were associated with a reduced NDVI, reflecting lower vegetation productivity.

Lastly, we investigated the relationship between the NDVI and NPP, which measures the rate at which vegetation produces biomass through photosynthesis minus losses for respiration. The correlation showed a Pearson coefficient of 0.95 (Figure 8e,f), indicating that the NDVI is likely to be a robust indicator of plant productivity and biomass production for this region, with the caveat that the NPP estimation also uses satellite vegetation estimates in the model formulation.

5. Conclusions

In conclusion, our study provides the first integrated, data-driven assessment of vegetation dynamics in Thi-Qar Governorate in southern Iraq, clearly quantifying the relative roles of hydrological and climatic drivers across different land cover types. The analysis reveals that land degradation is widespread but spatially heterogeneous, with over half (56.5%) of the region experiencing declining vegetation productivity between 2001 and 2022, concentrated in the southern and western parts. However, the northern parts of the marshes and the center of the study area presented a small positive trend in vegetation productivity due to consistent water availability. A key mechanistic finding is that streamflow exerts a stronger influence on vegetation cover than precipitation or temperature in this arid and semi-arid riparian system. Multiple regression and partial correlation analyses consistently identified streamflow as the most significant positive driver of the NDVI, particularly in agriculturally productive zones such as croplands and arable lands, where it explained the majority of vegetation variability. This underscores that human-managed water resources—not rainfall—are the primary controllable factor governing vegetation resilience in Thi-Qar. However, the impact of these three factors on the NDVI was weak for bare areas and sand dunes. The strong observed link between streamflow and the NDVI, coupled with weak correlations in non-vegetated areas, suggests that targeted hydrological interventions could rapidly improve vegetation cover in vulnerable but recoverable landscapes, whereas severely degraded bare areas and dunes may require more intensive rehabilitation.

In summary, our results identify the degraded areas of this region of Iraq, which is vulnerable to both climate change and management policies, and highlight the factors that influence these areas. By quantifying the dominant role of streamflow over climatic variables, the study offers critical information for creating policies that support LULC planning and water management. This research supports global efforts in arid and semi-arid regions facing similar challenges, such as the Sahel, the southwestern United States, and the MENA region.

Author Contributions: Conceptualization, A.A., P.N., J.R. and I.B.; methodology, A.A.; software, A.A.; validation, A.A., P.N. and I.B.; formal analysis, A.A. and P.N.; investigation, A.A. and P.N.; resources, P.N. and J.R.; data curation, A.A.; writing—original draft preparation, A.A.; writing—review and editing, P.N., I.B., J.R. and S.L.; visualization, A.A.; supervision, P.N., J.R. and I.B.; project administration, P.N., J.R. and I.B.; funding acquisition, P.N. All authors have read and agreed to the published version of the manuscript.

Funding: Prof. North acknowledges support from the NERC National Centre for Earth Observation (NERC grant reference number NE/Y006216/1).

Data Availability Statement: The data supporting this study's findings are available on request from the corresponding author. Google Earth Engine provided access to satellite imagery under institutional agreements.

Acknowledgments: We would like to express gratitude to the Iraqi Ministry of Justice for funding this research and their invaluable support and encouragement. North acknowledges support from the NERC National Centre for Earth Observation (NERC grant reference number NE/Y006216/1). Furthermore, we would like to thank the Google Earth Engine development team for granting storage memory and computational resources.

Conflicts of Interest: The authors declare that they have no competing financial or personal interests that could influence the results of this study.

Abbreviations

GEE	Google Earth Engine
MODIS	Moderate-Resolution Imaging Spectroradiometer
NDVI	Normalized Difference Vegetation Index
LST	Land Surface Temperature
ET	Evapotranspiration
NPP	Net Primary Productivity
MENA	Middle East–North Africa
DDP	Dahlem Desertification Paradigm
RUE	Rain Use Efficiency
UNDB	United Nations Development Business
CHIRPS	Climate Hazards Group InfraRed Precipitation with Station
WaPOR	Water Productivity through Open access Remotely sensed derived data
FAO	Food and Agriculture Organization

References

1. Hamed, M.M.; Al-Hasani, A.A.J.; Nashwan, M.S.; Sa'adi, Z.; Shahid, S. Assessing the Growing Threat of Heat Stress in the North Africa and Arabian Peninsula Region Connected to Climate Change. *J. Clean. Prod.* **2024**, *447*, 141639. [CrossRef]
2. Adamo, N.; Al-Ansari, N.; Sissakian, V.; Fahmi, K.J.; Abed, S.A. Climate Change: Droughts and Increasing Desertification in the Middle East, with Special Reference to Iraq. *Engineering* **2022**, *14*, 235–273. [CrossRef]
3. Djebou, D.C.S.; Singh, V.P.; Frauenfeld, O.W. Vegetation Response to Precipitation Across the Aridity Gradient of the Southwestern United States. *J. Arid Environ.* **2015**, *115*, 35–43. [CrossRef]
4. Cherlet, M.; Hutchinson, C.; Reynolds, J.; Hill, J.; Sommer, S.; von Maltitz, G. *World Atlas of Desertification*; Publications Office of the European Union: Luxembourg, 2018; JRC111155. [CrossRef]
5. Rivera-Marin, D.; Dash, J.; Ogutu, B. The Use of Remote Sensing for Desertification Studies: A Review. *J. Arid Environ.* **2022**, *206*, 104829. [CrossRef]
6. Almalki, R.; Khaki, M.; Saco, P.M.; Rodriguez, J.F. Monitoring and Mapping Vegetation Cover Changes in Arid and Semi-arid Areas Using Remote Sensing Technology: A Review. *Remote Sens.* **2022**, *14*, 5143. [CrossRef]
7. Piao, S.L.; Fang, J.Y.; Zhou, L.M.; Guo, Q.H.; Henderson, M.; Ji, W.; Li, Y.; Tao, S. Interannual Variations of Monthly and Seasonal Normalized Difference Vegetation Index (NDVI) in China From 1982 to 1999. *J. Geophys. Res. Atmos.* **2003**, *108*, 4401. [CrossRef]
8. Chen, X.; Wang, Y.; Chen, Y.; Fu, S.; Zhou, N. NDVI-based Assessment of Land Degradation Trends in Balochistan, Pakistan, and Analysis of the Drivers. *Remote Sens.* **2023**, *15*, 2388. [CrossRef]

9. Los, S.O.; Justice, C.O.; Tucker, C.J. A global 1° × 1° NDVI Dataset for Climate Studies Derived from the GIMMS Continental NDVI Data. *Int. J. Remote Sens.* **1994**, *15*, 3493–3518. [CrossRef]
10. North, P.R.J. Estimation of fAPAR, LAI, and Vegetation Fractional Cover From ATSR-2 Imagery. *Remote Sens. Environ.* **2002**, *80*, 114–121. [CrossRef]
11. Symeonakis, E.; Drake, N. Monitoring Desertification and Land Degradation Over Sub-Saharan Africa. *Int. J. Remote Sens.* **2004**, *25*, 573–592. [CrossRef]
12. Huber-Sannwald, E.; Maestre, F.T.; Herrick, J.E.; Reynolds, J.F. Ecohydrological Feedbacks and Linkages Associated with Land Degradation: A Case Study from Mexico. *Hydrol. Process.* **2006**, *20*, 3395–3411. [CrossRef]
13. Aladejana, O.O.; Salami, A.T.; Adetoro, O.I.O. Hydrological Responses to Land Degradation in the Northwest Benin Owena River Basin, Nigeria. *J. Environ. Manag.* **2018**, *225*, 300–312. [CrossRef] [PubMed]
14. Rahman, G.; Farooq, U.; Jung, M.-K.; Kwon, H.-H. Spatiotemporal Vegetation Dynamics in South Asia (2001–2023): Roles of Climate and Anthropogenic Activities. *Geosci. Lett.* **2025**, *12*, 31. [CrossRef]
15. Anwer, H.A.; Mohamed, T.; Hassan, A. Assessing Vegetation Dynamics in Al Jazirah, Sudan using NDVI-based Remote Sensing Techniques. *J. Saudi Soc. Agric. Sci.* **2025**, *24*, 18. [CrossRef]
16. Moses, O.; Blamey, R.C.; Reason, C.J. Relationships Between NDVI, River Discharge and Climate in the Okavango River Basin Region. *Int. J. Climatol.* **2022**, *42*, 691–713. [CrossRef]
17. Zhang, H.; Li, L.; Zhao, X.; Chen, F.; Wei, J.; Feng, Z.; Hou, T.; Chen, Y.; Yue, W.; Shang, H.; et al. Changes in Vegetation NDVI and its Response to Climate Change and Human Activities in the Ferghana Basin From 1982 to 2015. *Remote Sens.* **2024**, *16*, 1296. [CrossRef]
18. Chen, S.; Ji, L.; Li, P.; Zhang, Y.; Tang, H.; Liu, X.; Wang, J. The Spatio-Temporal Variation of Vegetation and its Driving Factors During the Recent 20 Years in Beijing. *Remote Sens.* **2024**, *16*, 851. [CrossRef]
19. Cheng, Y.; He, G.; Luo, J.; Gu, H.; Zhang, Z.; Liu, Y. Effects of Climate Change on Temperature Sensitivity of Vegetation Growth in the Huang–Huai–Hai Plain: Spatial–Temporal Dynamics and Ecological Adaptability. *Remote Sens.* **2024**, *16*, 4024. [CrossRef]
20. Al-Obaidi, J.R.; Allawi, M.Y.; Al-Taie, B.S.; Alobaidi, K.H.; Al-Khayri, J.M.; Abdullah, S.; Ahmad-Kamil, E.I. The Environmental, Economic, and Social Development Impact of Desertification in Iraq: A Review on Desertification Control Measures and Mitigation Strategies. *Environ. Monit. Assess.* **2022**, *194*, 440. [CrossRef]
21. Ethaib, S.; Zubaidi, S.L.; Al-Ansari, N. Evaluation Water Scarcity Based on GIS Estimation and Climate-Change Effects: A Case Study of Thi-Qar Governorate, Iraq. *Cogent Eng.* **2022**, *9*, 2075301. [CrossRef]
22. Sun, P.; Liu, S.; Jiang, H.; Lü, Y.; Liu, J.; Lin, Y.; Liu, X. Hydrologic Effects of NDVI Time Series in a Context of Climatic Variability in an Upstream Catchment of the Minjiang River. *J. Am. Water Resour. Assoc.* **2008**, *44*, 1132–1143. [CrossRef]
23. Jia, M.; Hu, S.; Hu, X.; Long, Y. Response Mechanism of Annual Streamflow Decline to Vegetation Growth and Climate Change in the Han River Basin, China. *Forests* **2023**, *14*, 2132. [CrossRef]
24. Al-Maliki, L.A.; Al-Mamoori, S.K.; Al-Ansari, N.; El-Tawel, K.; Comair, F.G. Climate Change Impact on Water Resources of Iraq: A review. *IOP Conf. Ser. Earth Environ. Sci.* **2022**, *1120*, 012025. [CrossRef]
25. Ali, H.M.; Shakir, R.R. Geotechnical Map of Thi Qar Governorate Using Geographical Information Systems. *Mater. Today Proc.* **2022**, *60*, 1286–1296. [CrossRef]
26. Al-Ansari, N.; Abbas, N.; Laue, J.; Knutsson, S. Water scarcity: Problems and Possible Solutions. *J. Earth Sci. Geotech. Eng.* **2021**, *11*, 243–315. [CrossRef]
27. Didan, K. *MODIS/Terra Vegetation Indices 16-Day L3 Global 250 m SIN Grid V061*; NASA Land Processes Distributed Active Archive Center: Sioux Falls, SD, USA, 2021. [CrossRef]
28. Alemayehu, B.; Suarez-Minguez, J.; Rosette, J.; Khan, S.A. Vegetation Trend Detection Using Time-Series Satellite Data as Ecosystem Condition Indicators for Analysis in the Northwestern Highlands of Ethiopia. *Remote Sens.* **2023**, *15*, 5032. [CrossRef]
29. Funk, C.; Peterson, P.; Landsfeld, M.; Pedreros, D.; Verdin, J.; Shukla, S.; Michaelsen, J. The Climate Hazards Infrared Precipitation with Stations—A New Environmental Record for Monitoring Extremes. *Sci. Data* **2015**, *2*, 150066. [CrossRef]
30. Enyew, F.B.; Wassie, S.B. Rainfall Trends and Spatiotemporal Patterns of Meteorological Drought in Menna Watershed, Northwestern Ethiopia. *Heliyon* **2024**, *10*, e26038. [CrossRef]
31. FAO. *WaPOR V2 Database Methodology: Remote Sensing for Water Productivity*; FAO: Rome, Italy, 2020. Available online: https://developers.google.com/earth-engine/datasets/catalog/FAO_WAPOR_2_L1_NPP_D (accessed on 15 February 2025).
32. Liu, X.; Lai, Q.; Yin, S.; Bao, Y.; Tong, S.; Adiya, Z.; Gao, R. Spatio-Temporal Patterns and Control Mechanism of Ecosystem Carbon Use Efficiency Across the Mongolian Plateau. *Sci. Total Environ.* **2024**, *907*, 167883. [CrossRef]
33. Demessie, S.F.; Woldeyohannes, M. Evaluation of Water Productivity of Smallholder Irrigation Along a Sand River, in the Maigobo Watershed of Northern Ethiopia. *Environ. Chall.* **2024**, *14*, 100801. [CrossRef]
34. Liu, Y.; Wang, Y.; Yang, Y.; Jiang, H.; Jing, W. Impacts of Hydrometeorological Controls on Vegetation Productivity: Evidence from Satellite Observations and Reanalysis. *Ecol. Indic.* **2024**, *161*, 111976. [CrossRef]

35. Running, S.; Mu, Q.; Zhao, M. *MODIS/Terra Net Evapotranspiration 8-Day L4 Global 500 m SIN Grid V061*; NASA LP DAAC: Sioux Falls, SD, USA, 2021. [CrossRef]
36. Mu, Q.; Zhao, M.; Running, S.W. Improvements to a MODIS Global Terrestrial Evapotranspiration Algorithm. *Remote Sens. Environ.* **2011**, *115*, 1781–1800. [CrossRef]
37. Mu, Q.; Zhao, M.; Running, S.W. *MODIS Global Terrestrial Evapotranspiration (ET) Product (MOD16A2/A3) Algorithm Theoretical Basis Document*; NASA: Washington, DC, USA, 2013.
38. Wan, Z.; Hook, S.; Hulley, G. *MODIS/Terra Land Surface Temperature/Emissivity Daily L3 Global 1 km SIN Grid V061*; NASA LP DAAC: Sioux Falls, SD, USA, 2021. [CrossRef]
39. Yu, W.; Nan, Z.; Wang, Z.; Chen, H.; Wu, T.; Zhao, L. An Effective Interpolation Method for MODIS Land Surface Temperature on the Qinghai–Tibet plateau. *IEEE J. Sel. Top. Appl. Earth Obs. Remote Sens.* **2015**, *8*, 4539–4550. [CrossRef]
40. Mann, H.B. Nonparametric Tests Against Trend. *Econometrica* **1945**, *13*, 245–259. [CrossRef]
41. Kendall, M.G. *Rank Correlation Methods*, 4th ed.; Griffin: London, UK, 1975.
42. Colditz, R.R.; Ressl, R.A.; Bonilla-Moheno, M. Trends in 15-Year MODIS NDVI Time Series for Mexico. In Proceedings of the 8th International Workshop on the Analysis of Multitemporal Remote Sensing Images, Annecy, France, 22–24 July 2015. [CrossRef]
43. Mohammad, L.; Mondal, I.; Bandyopadhyay, J.; Pham, Q.B.; Nguyen, X.C.; Dinh, C.D.; Al-Quraishi, A.M.F. Assessment of Spatio-Temporal Trends of Satellite-Based Aerosol Optical Depth Using Mann–Kendall Test and Sen's Slope Estimator Model. *Geomatics Nat. Hazards Risk* **2022**, *13*, 1270–1298. [CrossRef]
44. Luo, N.; Mao, D.; Wen, B.; Liu, X. Climate Change Affected Vegetation Dynamics in the Northern Xinjiang of China: Evaluation by SPEI and NDVI. *Land* **2020**, *9*, 90. [CrossRef]
45. Wang, J.; Fan, Y.; Yang, Y.; Zhang, L.; Zhang, Y.; Li, S.; Wei, Y. Spatial-Temporal Evolution Characteristics and Driving Force Analysis of NDVI in the Minjiang River Basin, China, From 2001 to 2020. *Water* **2022**, *14*, 2923. [CrossRef]
46. Li, C.; Jia, X.; Zhu, R.; Mei, X.; Wang, D.; Zhang, X. Seasonal Spatiotemporal Changes in the NDVI and Its Driving Forces in Wuliangsu Lake Basin, Northern China from 1990 to 2020. *Remote Sens.* **2023**, *15*, 2965. [CrossRef]
47. Ke, H.; Liang, L.; Tian, M.; Wang, M.; Yuan, C.; Gao, Y. Assessing Vegetation Dynamics and Influencing Factors in Northwest China's Arid Regions: A Spatiotemporal Analysis Using NDVI (2000–2020). *Acta Geophys.* **2025**, *73*, 3405–3424. [CrossRef]
48. Neeti, N.; Eastman, J.R. A Contextual Mann-Kendall Approach for the Assessment of Trend Significance in Image Time Series. *Trans. GIS* **2011**, *15*, 599–611. [CrossRef]
49. Baig, M.R.I.; Shahfahad; Naikoo, M.W.; Ansari, A.H.; Ahmad, S.; Rahman, A. Spatio-Temporal Analysis of Precipitation Pattern and Trend Using Standardized Precipitation Index and Mann–Kendall Test in Coastal Andhra Pradesh. *Model. Earth Syst. Environ.* **2022**, *8*, 2733–2752. [CrossRef]
50. Shi, L.; Fan, H.; Yang, L.; Jiang, Y.; Sun, Z.; Zhang, Y. NDVI-Based Spatial and Temporal Vegetation Trends and Their Response to Precipitation and Temperature Changes in the Mu Us Desert From 2000 to 2019. *Water Sci. Technol.* **2023**, *88*, 430–442. [CrossRef] [PubMed]
51. Wei, Y.; Sun, S.; Liang, D.; Jia, Z. Spatial–Temporal Variations of NDVI and its Response to Climate in China from 2001 to 2020. *Int. J. Digit. Earth* **2022**, *15*, 1463–1484. [CrossRef]
52. Zhang, W.; Wang, Z.; Meng, M.; Li, T.; Guo, J.; Sun, D.; Shen, X. Long-Term NDVI Trends and Vegetation Resilience in a Seismically Active Debris Flow Watershed: A Case Study from the Wenchuan Earthquake Zone. *Sustainability* **2025**, *17*, 5081. [CrossRef]
53. Mnb, H.A.; Hanifa, S.N. Spatio-Temporal NDVI Changes of Mangrove Forest in West Bangkalan Using High Resolution Imagery. *E3S Web Conf.* **2024**, *499*, 01032. [CrossRef]
54. Best, D.J.; Roberts, D.E. Algorithm AS 89: Upper tail probabilities of Spearman's rho. *J. R. Stat. Soc. Ser. C* **1975**, *24*, 377–379. [CrossRef]
55. Yan, J.; Zhang, G.; Ling, H.; Han, F. Comparison of Time-Integrated NDVI and Annual Maximum NDVI for Assessing Grassland Dynamics. *Ecol. Indic.* **2022**, *136*, 108611. [CrossRef]
56. Han, W.; Chen, D.; Li, H.; Chang, Z.; Chen, J.; Ye, L.; Wang, Z. Spatiotemporal Variation of NDVI in Anhui Province from 2001 to 2019 and Its Response to Climatic Factors. *Forests* **2022**, *13*, 1643. [CrossRef]
57. Sheskin, D.J. *Handbook of Parametric and Nonparametric Statistical Procedures*, 5th ed.; CRC Press: Boca Raton, FL, USA, 2011.
58. Cohen, J.; Cohen, P.; West, S.G.; Aiken, L.S. *Applied Multiple Regression/Correlation Analysis for the Behavioral Sciences*; Routledge: New York, NY, USA, 2013. [CrossRef]
59. Xin, Z.; Xu, J.; Zheng, W. Spatiotemporal Variations of Vegetation Cover on the Chinese Loess Plateau (1981–2006): Impacts of Climate Changes and Human Activities. *Sci. China Ser. D* **2008**, *51*, 67–78. [CrossRef]
60. Hassan, H.M.; Dakheel, H.S. NDVI-Based Vegetation Cover Change in Thi-Qar Governorate. *Biol. Sci.* **2023**, *13*, 72–84.
61. Azeez, M.H.; Al-Sharaa, H.M.J.; Ziboon, A.R.T. Time Series Analysis of Vegetation Index and Land Degradation Assessment in Dhi Qar Governorate (Iraq). *J. Eng. Sustain. Dev.* **2025**, *29*, 634–642. [CrossRef]
62. Lasaponara, R.; Abate, N.; Fattore, C.; Aromando, A.; Cardettini, G.; Di Fonzo, M. On the Use of Sentinel-2 NDVI Time Series and Google Earth Engine to Detect Land-Use/Land-Cover Changes in Fire-Affected Areas. *Remote Sens.* **2022**, *14*, 4723. [CrossRef]

63. Ghorbanian, A.; Mohammadzadeh, A.; Jamali, S. Linear and Non-Linear Vegetation Trend Analysis Throughout Iran Using Two Decades of MODIS NDVI Imagery. *Remote Sens.* **2022**, *14*, 3683. [CrossRef]
64. Al-Tameemi, N.; Xuexia, Z.; Shahzad, F.; Mehmood, K.; Linying, X.; Zhou, J. From Trends to Drivers: Vegetation Degradation and Land-Use Change in Babil and Al-Qadisiyah, Iraq (2000–2023). *Remote Sens.* **2025**, *17*, 3343. [CrossRef]
65. Shafizadeh-Moghadam, H.; Khazaei, M.; Alavipanah, S.K.; Weng, Q. Google Earth Engine for Large-Scale Land Use and Land Cover Mapping: An Object-Based Classification Approach Using Spectral, Textural and Topographical Factors. *GISci. Remote Sens.* **2021**, *58*, 914–928. [CrossRef]
66. Nama, A.H.; Alwan, I.A.; Pham, Q.B. Climate Change and Future Challenges to the Sustainable Management of the Iraqi Marshlands. *Environ. Monit. Assess.* **2024**, *196*, 35. [CrossRef]
67. Albarakat, R.; Lakshmi, V.; Tucker, C.J. Using Satellite Remote Sensing to Study the Impact of Climate and Anthropogenic Changes in the Mesopotamian Marshlands, Iraq. *Remote Sens.* **2018**, *10*, 1524. [CrossRef]
68. Şarlak, N.; Mahmood Agha, O.M. Spatial and Temporal Variations of Aridity Indices in Iraq. *Theor. Appl. Climatol.* **2018**, *133*, 89–99. [CrossRef]
69. Ugbaje, S.U.; Bishop, T.F. Hydrological Control of Vegetation Greenness Dynamics in Africa: A Multivariate Analysis Using Satellite Observed Soil Moisture, Terrestrial Water Storage and Precipitation. *Land* **2020**, *9*, 15. [CrossRef]
70. Ukkola, A.M.; De Kauwe, M.G.; Roderick, M.L.; Burrell, A.; Lehmann, P.; Pitman, A.J. Annual Precipitation Explains Variability in Dryland Vegetation Greenness Globally but not Locally. *Glob. Change Biol.* **2021**, *27*, 4367–4380. [CrossRef]
71. Al-Bakri, J.T.; Salahat, M.; Suleiman, A.; Suifan, M.; Hamdan, M.R.; Khresat, S.; Kandakji, T. Impact of Climate and Land Use Changes on Water and Food Security in Jordan: Implications for Transcending "The Tragedy of the Commons". *Sustainability* **2013**, *5*, 724–748. [CrossRef]
72. Salman, S.A.; Shahid, S.; Ismail, T.; Chung, E.S.; Al-Abadi, A.M. Long-Term Trends in Daily Temperature Extremes in Iraq. *Atmos. Res.* **2017**, *198*, 97–107. [CrossRef]
73. Kadhim, S.S. Desertification and the Role of Changing Temperature and Rainfall Trends in Southern Iraq. *J. Al-Muthanna Agric. Sci.* **2024**, *11*, 1–9. [CrossRef] [PubMed]
74. Berdugo, M.; Delgado-Baquerizo, M.; Soliveres, S.; Hernández-Clemente, R.; Zhao, Y.; Gaitán, J.J.; Maestre, F.T. Global ecosystem thresholds driven by aridity. *Science* **2020**, *367*, 787–790. [CrossRef] [PubMed]
75. Feldman, A.F.; Short Gianotti, D.J.; Dong, J.; Trigo, I.F.; Salvucci, G.D.; Entekhabi, D. Tropical Surface Temperature Response to Vegetation Cover Changes and the Role of Drylands. *Glob. Change Biol.* **2023**, *29*, 110–125. [CrossRef] [PubMed]
76. Birtwistle, A.N.; Laituri, M.; Bledsoe, B.; Friedman, J.M. Using NDVI to Measure Precipitation in Semi-Arid Landscapes. *J. Arid Environ.* **2016**, *131*, 15–24. [CrossRef]
77. Conant, R.T.; Paustian, K.; Elliott, E.T. Grassland Management and Conversion into Grassland: Effects on Soil Carbon. *Ecol. Appl.* **2001**, *11*, 343–355. [CrossRef]
78. Al-Madhhachi, A.S.T.; Rahi, K.A.; Leabi, W.K. Hydrological Impact of Ilisu Dam on Mosul Dam; the River Tigris. *Geosciences* **2020**, *10*, 120. [CrossRef]
79. FAO. *AQUASTAT Main Database*; FAO: Rome, Italy, 2016. Available online: http://www.fao.org/nr/water/aquastat/data/query/index.html?lang=en (accessed on 10 February 2025).
80. Gleick, P.; Iceland, C.; Trivedi, A. *Ending Conflicts over Water*; Pacific Institute: Oakland, CA, USA, 2020.
81. Jia, L.; Shang, H.; Hu, G.; Menenti, M. Phenological Response of Vegetation to Upstream River Flow in the Heihe Rive Basin by Time Series Analysis of MODIS Data. *Hydrol. Earth Syst. Sci.* **2011**, *15*, 1047–1064. [CrossRef]
82. Maselli, F.; Chiesi, M.; Angeli, L.; Fibbi, L.; Rapi, B.; Romani, M.; Battista, P. An Improved NDVI-Based Method to Predict Actual Evapotranspiration of Irrigated Grasses and Crops. *Agric. Water Manag.* **2020**, *233*, 106077. [CrossRef]
83. Poudel, U.; Stephen, H.; Ahmad, S. Evaluating Irrigation Performance and Water Productivity Using EEFlux ET and NDVI. *Sustainability* **2021**, *13*, 7967. [CrossRef]